Rowe Mark D. (Orcid ID: 0000-0002-0852-3346)
Anderson Eric J (Orcid ID: 0000-0001-5342-8383)

Predicting larval alewife transport in Lake Michigan using hydrodynamic and Lagrangian particle dispersion models

Mark D. Rowe*[1], Sara E. Prendergast[2], Karen M. Alofs[3], David B. Bunnell[4], Edward S. Rutherford[2], and Eric J. Anderson[5]

[1]NOAA Great Lakes Environmental Research Laboratory, 4840 S. State Rd, Ann Arbor, MI. 48108

[2]Formerly, University of Michigan School for Environment and Sustainability, Dana Bldg, 440 Church St., Ann Arbor, MI. 48109.

[3]University of Michigan School for Environment and Sustainability, Dana Bldg, 440 Church St., Ann Arbor, MI. 48109

[4]US Geological Survey Great Lakes Science Center, 1451 Green Rd, Ann Arbor, MI. 48105

[5]Colorado School of Mines, Civil and Environmental Engineering, 1500 Illinois St, Golden, CO; formerly, NOAA Great Lakes Environmental Research Laboratory

* Corresponding author: mark.rowe@noaa.gov

Running head Predicting larval alewife transport

Abstract

Several species of fish in large lake and marine environments have a pelagic larval stage, and are subject to variable transport that can ultimately regulate survival and recruitment success. Alewife, *Alosa pseudoharengus*, are subject to transport by complex coastal currents during their

This is the author manuscript accepted for publication and has undergone full peer review but has not been through the copyediting, typesetting, pagination and proofreading process, which may lead to differences between this version and the Version of Record. Please cite this article as doi: 10.1002/lno.12186

pelagic larval stage (~30 days). We assessed backward-trajectory simulations, consisting of a Lagrangian particle dispersion model linked to the Finite Volume Community Ocean Model, to estimate likely hatch locations of aged larval alewife collected from locations on both the eastern and western sides of Lake Michigan during July 2015. We used four deployments of three satellite-tracked drifter buoys in coastal waters to assess model skill in estimating the origin of a drifter from its final location. We found that the trajectories of drifters varied greatly, depending on wind events and associated coastal transport processes, including upwelling/downwelling and coastal jet currents. In two of twelve cases, the backward trajectory simulations failed to predict the drifter origin, associated with transport of 170 km in a narrow coastal jet current. In the remaining ten cases, the known drifter origin was within 3.5 km of the spatial patch of predicted possible origins for a scenario of horizontal diffusivity (188 $m^2 s^{-1}$) consistent with the offshore model grid resolution. Modeled backward trajectories estimated that alewife originated from the same side of the lake where they were collected, within ~100 km of the collection site. Our paper demonstrates the utility of hydrodynamic models to estimate a region of origin for aged larval fish.

Introduction

Research into the physical and biological factors influencing growth and survival of fish with pelagic early life stages has improved understanding of fish recruitment in marine systems, and similar research is being emphasized in the Laurentian Great Lakes (Ludsin et al. 2014; Pritt et al. 2014). This new emphasis is timely given that the ecosystems of the Great Lakes have changed with the introduction of invasive dreissenid mussels, which have caused declines in pelagic primary production (Rowe et al. 2015; Vanderploeg et al. 2010) and potentially even prey fish populations (Bunnell et al. 2014). Climate change also is influencing stratification patterns (Anderson et al. 2021; Kraemer et al. 2015) and wind patterns (Desai et al. 2009), which can influence the transport of larval fish. Several studies have indicated the importance of upwelling and complex coastal currents in the dispersion of larval fish in Lake Michigan (Heufelder et al. 1982; Höök et al. 2007; Nash and Geffen 1991), but linking growth and survival to specific locations and transport scenarios has been hindered by lack of knowledge regarding the origins and trajectories of larval fish prior to capture.

Alewife (*Alosa psuedoharengus*) is an economically important prey fish in Lake Michigan. Initially an unwelcome invasive species to the Great Lakes in the 1950s and 1960s, alewife became the primary food source for stocked Pacific salmonids, supporting a multi-billion dollar recreational fishery (Dettmers et al. 2012). Total prey fish biomass, including alewife, has declined since the early 1970s in Lake Michigan (Bunnell et al. 2020), and there is growing concern that the alewife population will collapse as it did in Lake Huron in 2003 (Dunlop and Riley 2013; Riley et al. 2008). In Lake Huron, predation pressure from salmonids and lack of food availability from competition with the invasive dreissenid mussels led to the collapse of

alewife (He et al. 2014; Kao et al. 2016). Shortly thereafter, Chinook salmon populations collapsed (Johnson et al. 2010), with very limited evidence of a recovery (Clark Jr et al. 2017). To protect Lake Michigan against a similar outcome, managers seek to match the predator demand of salmonids with variable alewife population that may also be influenced by changes in lower trophic levels (Bunnell et al. 2018; Eggold et al. 2018; Eppehimer et al. 2019). Understanding the mechanisms underlying variable alewife recruitment would help both inform agency stocking decisions and improve stakeholder understanding of why stocking may need to be modified.

For fish that spawn in shallow, nearshore areas, including alewife (Withers 2015), the combined effect of nearshore currents and offshore circulation patterns control the fate of larval fish (Höök et al. 2006). The Great Lakes are comparable to coastal marine habitats in size, and share transport processes influenced by density stratification and the Earth's rotation. However, without a strong tidal effect, transport processes are primarily wind driven (Csanady 1975; Rao and Schwab 2007). Currents offshore are relatively weak, and exhibit features of topographic gyres, a result of wind stress acting on a bowl-shaped bathymetry (Csanady 1975). One dominant feature in offshore currents during the stratified season is the nearly circular motions caused by Poincare waves, an oscillation of the thermocline balanced by the Coriolis force, and having a period near the inertial period of 17 hours at the latitude of Lake Michigan (Choi et al. 2015; Csanady 1975; Rao and Schwab 2007). In the coastal boundary layer, ~5-10 km from the coast, bottom friction and the steering effect of the shore have a dominant influence on currents (Rao and Schwab 2007). Relatively strong currents occur near and are parallel to the coast, the result of wind stress acting on a shallow water column. These currents, known as coastal jets, can undergo sudden reversals due to changing wind direction or internal waves (Csanady 1975).

During the stratified season, a second dominant feature is coastal upwelling and/or downwelling in the coastal boundary layer. The nearshore region affected by upwelling is on the scale of the internal Rossby radius of deformation, ~3-5 km in the case of Lake Michigan (Rao and Schwab 2007). In small lakes, not influenced by Earth's rotation, wind stress directed from land to lake pushes surface water away from shore, resulting in elevation of the thermocline and shoreward movement of bottom water (upwelling), usually accompanied by depression of the thermocline (downwelling) on the opposite shore. In large lakes, of a size much greater than the internal Rossby radius, the surface current is modified by the Coriolis force, and directed to the right of the wind in the northern hemisphere; thus, wind parallel to the coast causes upwelling when the coast is to the left (Csanady 1975; Rao and Schwab 2007). In the case of Lake Michigan, a large lake, upwelling on the western shore is common during the summer, driven by dominant south and westerly wind components, while upwelling along the eastern shore was distinctly associated with northerly winds (Plattner et al. 2006). Plattner et al. (2006) reported limited success in statistical prediction of upwelling events from wind speed and direction, although the probability of upwelling increased with stronger winds (6-10 m s^{-1}), and numerical hydrodynamic models were recommended to predict the cumulative effect of variable wind speed and direction on upwelling.

Numerical hydrodynamic models are valuable tools for predicting currents and temperature in the Great Lakes, and substantial advancements have been made in their application. In one of the earliest attempts, Beletsky et al. (2007) applied the Princeton Ocean Model (POM) with a 2-km uniform grid and a Lagrangian particle dispersion (LPD) model to predict yellow perch trajectories after hatching in the southern basin of Lake Michigan and found that larval fish could move as far as the northern basin (approximately 320 km) with a drifting

stage lasting between 63 and 77 days. Brodnick et al. (2016) also used a similar POM model, but used backward trajectory simulations to estimate the hatch locations of known-age larval walleye sampled in Lake Erie. More recently, the Finite Volume Community Ocean Model (FVCOM) has been developed with an unstructured grid, which has the advantage of conforming to realistic shoreline morphology and attaining higher grid resolution in the coastal boundary layer. Anderson and Schwab (2013; 2017) applied FVCOM to Lake Michigan-Huron to simulate complex reversing currents in the Straits of Mackinac, which connect the two lakes. The same model was further developed into the National Oceanic and Atmospheric Administration (NOAA) Lake Michigan-Huron Operational Forecasting System (LMHOFS) with a grid resolution of 100-500 m along the coast, transitioning to 2.5 km mid-lake; LMHOFS has been recently assessed for its ability to simulate temperature and currents (Kelley et al. 2020; Peng et al. 2019). Previous studies have used an LPD model, driven by FVCOM output, to study transport of larval cod in the Gulf of Maine (Churchill et al. 2011; Huret et al. 2007). In contrast to the earlier LPD model used by Beletsky et al. (2007), the LPD model linked to FVCOM uses a random-walk vertical mixing scheme with vertically-varying turbulent diffusivity, which was shown by Rowe et al. (2016) to result in more accurate dispersion simulations than a 2D surface-only model in a Lake Erie harmful algal bloom forecast.

In this paper, we sought to assess the utility of hydrodynamic models with improved representation of nearshore areas (e.g., LMHOFS with an LPD) to simulate coastal boundary layer currents, and the origins of coastal drifters. The first objective was to determine whether these models can accurately predict the origins of satellite-tracked drifters deployed in nearshore Lake Michigan using backward-trajectory simulations. Following this model assessment, our second objective was to use the linked models to estimate the origins (i.e., hatch locations) of

known-aged pelagic larval alewife sampled in Lake Michigan to improve understanding of their current-driven advection.

Methods

Larval Alewife Collections

Larval alewife samples were collected during July 8-27, 2015 in Lake Michigan by the U. S. Geological Survey Great Lakes Science Center as part of the multi-agency Cooperative Science and Monitoring Initiative (Foley and Collingsworth 2018). Larval fish were sampled along eight nearshore to offshore transects with four each on the eastern and western sides: Frankfort, Ludington, Saugatuck, and St. Joseph in Michigan; Waukegan in Illinois; Racine, Manitowoc, and Sturgeon Bay in Wisconsin (see Figure 1). Three bathymetric depth sites (18-m, 46-m, and 91 or 110-m) were sampled along each transect. Both surface and oblique ichthyoplankton tows were performed at each site and all sampling was completed at night when alewife larvae move higher into the water column (Madenjian and Jude 1985). Further details of the collection methods are provided by Eppehimer et al. (2019).

Alewife Otolith Analysis

We used sagittal otoliths to estimate age of larval alewife as these are considered to be the most precise structure for this type of analysis (LaBay and Lauer 2006). Daily otolith growth increments have been previously used as a proxy for alewife age (Eppehimer et al. 2019; Höök et al. 2007). The first ring is likely laid on the second day of life (Essig and Cole 1986); thus, we added two to the number of increments counted to determine the age of the larval fish. We captured images of the otoliths using an imaging system (QICAM 12-bit; Teledyne QImaging,

Surrey, BC, Canada) and counted increments using image analysis software (Image-Pro Premier Version 9.0; Media Cybernetics, Inc., Rockville, Maryland). We observed otoliths under 1000x magnification (oil-immersed 100x objective lens; with 10x eyepiece lenses).

We conducted blind age estimates and compared them to those reported by Eppehimer et al. (2019). If our age estimate differed by more than one day from Eppehimer et al. (2019), a second analyst counted the rings, and if the estimate from the second analyst differed by more than a day from the reading by Eppehimer et al. (2019), the sample was omitted from the study. To ensure that sampled larvae were passive drifters, we excluded fish larger than 22 mm total length because the alewife larval stage lasts between 30-40 days and alewife $\leq$ 22 mm are most likely larvae (Klumb et al. 2003; Norden 1968). Twelve larvae > 22 mm were omitted, leaving a total of 297 larvae ranging in length from 4.8 to 22 mm, and in age from 5 to 34 days.

Satellite Tracked Drifting Buoys

We deployed satellite-tracked drifters on three separate occasions in 2018. In the first deployment, three drifters were released at 15-m, 45-m, and 110-m depth locations offshore of Muskegon, MI (herein M15, M45, and M110, respectively; Figure 1) on June 5 and retrieved June 12. In the second deployment, three drifters were released on June 27, with one released at M15 and two released 12 hours apart at M45. All drifters beached by July 4. For the third deployment, three drifters were released on July 18 at M15, M45, and, M110, and were retrieved on shore on August 5. All release dates were during periods when alewife larvae were likely present and passively drifting in the water column (Heufelder et al. 1982). We also analyzed data from three drifters deployed offshore of Muskegon, MI between the 15 and 45-m depth contours on June 30, 2015 by the University of Maryland (Mao and Xia 2020b), which remained in the

lake for approximately one month (https://www.nefsc.noaa.gov/drifter). All drifters in this study were designed after the "Eddie" drifter described by NOAA's Northeast Fishery Science Center (https://apps-nefsc.fisheries.noaa.gov/nefsc/emolt/driftdesign.html#Eddie), which is similar to the CODE drifter design (Davis 1985), but with floats only on the central column, not at the four corners. The drifter had a cruciform drogue extending 1 m below the surface with a weight and floats attached to the center column. An attached Global Positioning System (GPS) unit (SmartoneBLP; Globalstar, Chantilly, Virginia) at the top of the central column transmitted drifter position hourly in 2018 and every two hours in 2015. We interpreted drifter tracks, model temperature and currents with respect to observations of temperature, wind, and currents (acoustic Doppler current profiler, ADCP) from the NOAA buoy 45161 (www.glerl.noaa.gov/metdata/metReCON.html) located at the Muskegon 15-m station (Figure 1). The ADCP (Nortek AWAC 600 kHz) recorded a 10-minute vector average of data samples taken at 60s intervals. We estimated the effect of Stoke's drift (Webb and Fox-Kemper 2011) due to wind waves and leeway (Röhrs et al. 2012) on the drifter tracks using wind and wave observations at buoy 45161, and found the effects to be small in comparison to the direct effect of currents for all deployments (3-6% of total drift distance).

Hydrodynamic and trajectory modeling

The LMHOFS model (https://tidesandcurrents.noaa.gov/ofs/lmhofs/lmhofs.html) is an application of FVCOM (http://fvcom.smast.umassd.edu/); a three-dimensional oceanographic model that implements a numerical solution of the momentum, continuity, temperature, salinity, and density equations (Chen et al. 2003). The vertical dimension is defined using terrain following (sigma) coordinates with 20 uniformly-distributed layers. Data assimilation was not

used in LMHOFS. LMHOFS used hourly meteorological forcing from the NOAA High-Resolution Rapid Refresh (HRRR) model (Benjamin et al. 2016). The 3-km horizontal resolution of the HRRR model, which utilizes data assimilation, makes the model well-suited for simulation of winds in coastal environments (James et al. 2018).

The Lagrangian particle dispersion (LPD) model (Churchill et al. 2011; Huret et al. 2007; Rowe et al. 2016) is distributed as part of the FVCOM code package (http://fvcom.smast.umassd.edu/). A fixed time step of 600 s was used with a fourth-order Runge-Kutta scheme to integrate three-dimensional velocity components in calculation of trajectories. Velocities were interpolated using hourly output from FVCOM. We applied the model in a backward-trajectory mode, initiating the Lagrangian particles at the capture location of larval fish, or at the ending location of a drifter buoy, and running the model backward in time through the records of hydrodynamic output for a period representing the age of the oldest fish in a sample, or the buoy drift duration, in order to estimate the possible region of origin (i.e,. location of hatching) for larval fish in a sample, or initial location of the drifter buoy. We used a reflecting lateral boundary condition to prevent trajectories from traveling over land, and to prevent accumulation of Lagrangian particles along the shore. The model bathymetry and physical processes lacked sufficient detail in the surf zone and swash zone to simulate beaching of drifter buoys, so we limited simulations to the period prior to beaching, for drifters that beached. To represent the stochastic nature of drifter trajectories in turbulent flow, we initiated simulations with an ensemble of 1000 particles placed at the surface and ran simulations with random walk turbulent diffusivity routines to capture effects of sub-grid-scale turbulent motions. We simulated backward trajectories of drifter buoys using horizontal diffusivity and with vertical location fixed at the mid-depth of the drifter drogue (0.5 m). We simulated backward trajectories

of larval fish using both horizonal and vertical diffusivity. Vertical random walk diffusivity was implemented using vertically varying turbulent diffusivity output from FVCOM, a variable random walk time step was set to satisfy stability criteria, to prevent artificial accumulation of particles in low diffusivity areas (Rowe et al., 2016). Horizontal diffusivity (K_H) varies according to the model grid spacing (Δ), to represent the un-resolved turbulent motions. For example, in a solute dispersion experiment in coastal Lake Michigan, Thupaki et al. (2013) found that a K_H value of 5.6 m^2 s^{-1} was required to describe data from a dye release experiment in their 100-m resolution, uniform grid, model, and that value was closely approximated by the relation $K_H = 0.03\ \Delta^{1.15}$ (De Brauwere et al. 2011). Using the same relation, we estimated K_H in our unstructured grid model as 13 m^2 s^{-1} along the coast ($\Delta \approx 200$ m) and 188 m^2 s^{-1} mid-lake ($\Delta \approx$ 2000 m). To apply spatially-varying diffusivity in a LPD model, specific numerical methods must be used to avoid artificial accumulation of particles in low diffusivity areas (Hunter et al. 1993; Rowe et al. 2016). It was beyond the scope of this study, however, to modify the LPD model to accommodate spatially-varying K_H. To show the effect of the range of diffusivity appropriate to the range of grid spacing in our model, we ran two scenarios of backward trajectory simulations using K_H values of 13 m^2 s^{-1} and 188 m^2 s^{-1}.

The result of backward trajectory simulations was a spatial patch of likely origin locations. To visualize the patch, we plotted locations of the ensemble of Lagrangian particles at the time of the origin. To further limit predicted origin locations of larval fish to nearshore locations where alewife are likely to spawn, we defined the nearshore environment as the region between the shoreline and the 20-m bathymetric contour (Withers 2015), and origins predicted outside of the nearshore environment were noted for visualization.

We used satellite-tracked drifter buoy trajectories to assess the backward-trajectory modeling approach, under scenarios of horizontal diffusivity (K_H). We conducted backward trajectory simulations for the 12 drifter trajectories from the 2015 and 2018 releases. Recognizing that there is not a unique possible origin for a drifter due to the stochastic nature of turbulence, our predictions were in the form of a spatial patch of likely origin locations, and for a successful prediction, the observed drifter origin would be anywhere within the patch. Therefore, we defined a skill metric as the distance between the known drifter location and the patch of modeled likely locations, represented by the distance to the nearest Lagrangian particle.

Results

Current speeds from satellite-tracked drifter buoys averaged 0.17 m s^{-1}, with an interquartile range of 0.08-0.23 m s^{-1} (Figure 2). Current speeds varied across deployment dates. The slowest speeds occurred on the deployments of June 27 and July 18, 2018, with a mean of 0.08 m s^{-1} and interquartile range of 0.03-0.11. On the remaining deployment dates, the current speed averaged 0.15 m s^{-1} with an interquartile range of 0.06-0.21 m s^{-1}. Mean surface current speeds (and interquartile range) measured by the ADCP located at M15 in the month of July were 0.19 (0.11-0.27) m s^{-1} in 2018 and 0.11 (0.06-0.15) m s^{-1} in 2015. A majority of hourly observed drifter speeds (84%) were greater than a reported swimming speed of 0.03 m s^{-1} for larval alewife (Klumb et al. 2003).

Model-simulated currents, surface and bottom temperature, at the 15-m station offshore of Muskegon (Figure 1; M15) captured the main features of observed upwelling/downwelling and coastal jet currents, although there were errors in magnitude, direction, and the timing of events. Observed surface and bottom temperatures at M15 were used to identify upwelling or

downwelling conditions during drifter deployments (Figures 3 and 4). During upwelling events, surface temperature was low relative to preceding and subsequent periods, and bottom temperature was near the minimum value recorded (~ 5 °C), indicating elevation of the thermocline. In contrast, downwelling events were characterized by surface temperature near the maximum values recorded for the period, and elevated bottom temperature, consistent with deepening of the thermocline. During the first 2018 deployment, wind shifted from northerly to easterly, currents were relatively weak, and shifted from northerly to southerly, and temperature indicated upwelling (Figure 3). Model simulated currents were relatively weak and shifted from southerly to northerly, and simulated temperature indicated upwelling, consistent with observations, although there were errors in the magnitude and direction of currents. During the second 2018 deployment, wind shifted from easterly to southerly, current was relatively strong and northerly, and temperature indicated downwelling. Model simulated currents were mainly southerly and simulated temperature indicated downwelling, consistent with observations, but timing of the shift from northerly to southerly currents was delayed in the model. During the third 2018 deployment, wind was variable, currents shifted from northerly to southerly, and the upwelling initially present at deployment transitioned to downwelling. Model temperatures largely captured the upwelling and downwelling events, and shift from relatively strong northerly to southerly currents, but the timing of the shift in currents was delayed. The month-long drifter deployment in 2015 can be divided into an initial upwelling period followed by a downwelling period (Figure 4). During the upwelling period, wind was variable, but the strongest winds were northerly and currents were rotational. Model temperature indicated upwelling, and currents were relatively weak and rotational, consistent with observations, but at any given time there were errors between model and observed currents. During the downwelling

period, wind was often southerly, and currents were southerly. Modeled temperature indicated downwelling and currents were largely southerly, consistent with observations, but modeled currents shifted to northerly in the last five days of the deployment, contrary to observations.

Drifter trajectories differed greatly for upwelling versus downwelling conditions (Figures 5-7). During upwelling conditions, drifters exhibited looping trajectories that gradually moved offshore or parallel to shore, and with net movement to the south in most cases (Figure 5a, 5c, 7a). In contrast, during downwelling conditions drifters moved shoreward and were entrained into relatively strong coastal jet currents, which were oriented northward (Figure 6a, 6c, 7c). The complexity of the modeled coastal currents is shown in Figures 5-7 with vectors plotted at 1-km intervals along east-west transects. During the 2018-06-05 deployment, coastal currents were relatively weak and oriented offshore and to the north, consistent with net drifter movement, but in contrast to the shoreward orientation of the mean observed current at M15 (Figure 5b). During the 2018-07-18 deployment, there was a relatively strong southward current within 20-30 km of the coast, consistent with net southward movement of the drifters, but in contrast to the northward oriented current observed by ADCP at M15 (Figure 5d). While the model captured general features of the variable currents observed by ADCP during upwelling periods (Figure 3), errors in direction and the timing of current shifts resulted in the substantial apparent discrepancies when averaged over each upwelling period (Figure 5, white arrows). In the three downwelling periods, there was a northward oriented current within 10 km of the coast, with a southward and shoreward oriented current at 10-30 km from the coast, consistent with the shoreward then northward movement of the drifters, and consistent with the relatively strong northward current observed by ADCP at M15 (Figure 6b, 6d, 7d).

We used the drifter buoy tracks to assess backward-trajectory model skill in predicting the origin region of drifters from the known final location and drift duration. We conducted backward trajectory simulations for the 12 drifter deployments, using two scenarios of K_H values (13 and 188 $m^2 s^{-1}$), representative of the range of model grid resolution (~ 0.2 – 2 km). Two of the twelve drifters were retained within a narrow (~5 km from shore) coastal jet current, carrying the drifter along the contours of the coast for ~170 km, which was not possible for the backward-trajectory to fully reconstruct (Figure 8j,k). For the remaining ten drifters, use of $K_H = 188$ $m^2 s^{-1}$ resulted in the most accurate estimates of possible drifter origins (Figures 8 and 9); the known drifter origin was within 3.5 km of the spatial patch of predicted possible origins with $K_H = 188$ $m^2 s^{-1}$, in comparison to 19 km for $K_H = 13$ $m^2 s^{-1}$ (Figure 9). The distance between the known drifter origin and the spatial patch of predicted possible origins can be seen in Figure 8 by comparison of the red triangle location to the nearest blue or yellow points, and in Figure 9 by comparison of the y-axis values of the line endpoints.

We applied the backward trajectory model to predict origin locations of aged larval alewife. Predicted regions of possible hatch locations were similar for the two K_H scenarios, with $K_H = 188$ $m^2 s^{-1}$ resulting in slightly expanded regions (Figure 10). The predicted hatch locations of larval alewife collected in southwestern Lake Michigan were located within ~100 km to the south of the collection site (Figure 10a-f). In southeastern Lake Michigan, predicted hatch locations were more variable and disperse. In three cases, predicted hatch locations were within ~100 km to the north of the collection site (Figure 10h,k,i), while in the remaining three cases predicted hatch locations were within ~100 km north and south of the collection site (Figure 10g,j,l). In northern Lake Michigan, the predicted hatch location for the western collection site was located within ~100 km to the south, while the predicted hatch locations for the two eastern

collection sites were within ~100 km to the north (Figure 11). In all cases, the likely hatch region was on the same side of the lake as the collection site.

Discussion

Observed current speeds from satellite-tracked drifter buoys were greater than estimated larval alewife swimming speeds of 0.03 m s^{-1} for 84% of the hourly records, supporting the assumption that larval alewife are passive drifters. An average-sized alewife in our 2015 collections (i.e., 12 mm) likely only swims at a speed of 0.02-0.04 m s^{-1} (Klumb et al. 2003). These results suggest that larval alewife are highly susceptible to transport by currents in Lake Michigan, and that the collection of alewife larvae in offshore waters (e.g., Eppehimer et al. 2019; Weber et al. 2015) was most likely the result of advection from nearshore or riverine spawning habitats.

The trajectories of satellite-tracked drifter buoys varied widely across deployments, illustrating how, depending on wind and conditions, larval fish may be 1) retained in nearshore waters near their hatch locations, 2) transported offshore, or 3) transported to distant nearshore locations. For drifter deployments along the eastern shore, wind from the north and east produced upwelling and relatively gradual offshore transport with inertial oscillations. In contrast, wind from the south and west, associated with coastal downwelling, moved drifters shoreward and resulted in relatively rapid along-shore transport in coastal jet currents. These coastal jets were concentrated within 5-10 km from the coast (Figures 5-7), and while they affected a narrow nearshore zone, surface drifters were directed into, and retained in, that zone by shoreward movement of surface water associated with downwelling. Thus, the transport and

fate of larval fish within or out of the nearshore zone may be influenced by the coincidence of wind events with critical stages of development.

The backward trajectory simulations had some skill, although limited, in identifying the known initial position of drifter buoys, highlighting the challenges associated with this method. Mao and Xia (2020b) also assessed Lagrangian drifter simulations in Lake Michigan using satellite-tracked drifting buoys, but our approach differs from theirs in our inclusion of simulated dispersion, in our focus on use of backward trajectories to predict drifter origin locations, and in our use of high-resolution atmospheric forcing variables from the HRRR model. In a turbulent flow field, there is a multitude of possible initial positions for a drifter that could result in a given final position. By including random walk turbulence simulations in the model, this reality was represented by a patch of possible drifter initial positions. We used two scenarios of K_H (13 m^2 s^{-1} and 188 m^2 s^{-1}), representative of the 0.2-2 km resolution of our unstructured model grid (Thupaki et al. 2013), although diffusion values vary even when forcing and background conditions are similar (Choi et al. 2020). In addition to the real stochastic nature of turbulent flow, there are also inaccuracies in the model currents (Figures 3 and 4), and errors accumulate over the duration of a Lagrangian drift simulation. To further add to the challenge, drifter buoys are not entirely representative of the transport of dissolved or suspended constituents. While the backward trajectories showed limited skill (Figures 8 and 9), they were still able to provide bounds on the likely region of origin of drifters, which is useful given the limited number of tools available to identify hatch locations of larval fishes.

Some transport scenarios may be less amenable than others to simulation with the backward trajectory approach. For example, in Figure 8jk, the backward trajectory failed to simulate along-shore transport, even though a northward current along the eastern shore was

simulated by the model (Figure 7d), consistent with the drifter track. To the extent that a real or modeled drifter interacts with the coast due to shoreward-oriented currents in a forward trajectory, the drifter would be forced away from the coast by the currents in a backward trajectory, resulting in asymmetry between the forward and backward trajectories. In addition, the complex shoreline between the points north and south of Ludington, and interaction of gyre currents in the northern and southern basins in this region, may be challenging for the hydrodynamic model to simulate. Of the five scenarios modeled to track drifter movement between the two points north and south of Ludington (Figure 8defjk), the model predicted the particles to move offshore instead of following the alongshore coastal transport exhibited by the drifters.

The model suggests that larval alewife typically originated within ~100 km of their capture location and on the same side of the lake where they were captured. Beletsky et al. (2007) modeled larval yellow perch that hatched along the southwestern coast and found that in June and July drift trajectories often crossed to the eastern shore, and in August, they dispersed throughout the southern basin and into the eastern coastal region, although Beletsky et al. simulated longer drift periods (57-77 days) than in our study (11-34 days). While previous studies documented a cyclonic gyre circulation in southern Lake Michigan in long-term averaged model simulations (Beletsky and Schwab 2001; Xue et al. 2017), our predicted origins of larval alewife were consistent with anticyclonic circulation along the western shore, and variable circulation along the eastern shore. More recent studies have emphasized that circulation patterns are variable in response to wind events on shorter time scales, (days to weeks, Beletsky et al. 2017), and the importance of high-resolution models to resolve the coastal boundary layer (5-10 km), which can contain more variable and stronger currents than offshore (Mao and Xia 2020a;

Xue et al. 2017). Prior to being entrained into an offshore basin-scale gyre, coastal drifters must disperse out of the coastal boundary layer, and our simulations showed that downwelling events can direct drifters into the coastal boundary layer and result in rapid alongshore transport (Figures 6-7).

Potential nursery habitat can vary widely with respect to temperature and productivity (Höök et al. 2007; Stadig et al. 2020), which reinforces the potential criticality of larval alewife being transported into different regions. Alewife are known to spawn on both the eastern and western coasts of Lake Michigan, in addition to connected tributaries and drowned river mouths (Goodyear 1982). Not only can regions of the nearshore vary within the lake, for example the southeast region has relatively high nutrient loading owing to high nutrient inputs from several tributaries (Chapra and Dolan 2012), but whether larvae are transported from the nearshore to the offshore region also has been hypothesized to affect growth and survival of larvae in Lake Michigan (Dettmers et al. 2005; Weber et al. 2011; Weber et al. 2015).

Given our predictions of alewife transport, future research should duplicate our methods in other years to determine whether 2015 was an unusual year with respect to its prevailing winds and resultant currents (alongshore, upwelling, downwelling) or whether the proximity to the coastline of hatching is a more generalizable result. Furthermore, this approach could be coupled with a biological model that uses backward trajectories to predict zooplankton prey densities and temperatures experienced each day of "drift" to try and explain observed differences in growth rates and densities of larval alewife (see Eppehimer et al. 2019). Understanding the drivers of variation in recruitment for alewife remains a priority for fishery managers that adjust stocking rates of recreationally and commercially important salmonine species based on alewife recruitment and resultant population biomass.

Acknowledgements

Research was supported in part by U.S. Environmental Protection Agency and the Great Lakes Restoration Initiative. Sara Prendergast received support from the US Coast Guard and the Cooperative Institute for Great Lakes Research. Any use of trade, product, or firm names is for descriptive purposes only and does not imply endorsement by the U.S. Government. This is NOAA GLERL contribution 2006.

References

Anderson, E., and Schwab, D. 2013. Predicting the oscillating bi-directional exchange flow in the Straits of Mackinac. J. Great Lakes Res. **39**(4): 663-671.

Anderson, E.J., and Schwab, D.J. 2017. Meteorological influence on summertime baroclinic exchange in the Straits of Mackinac. J. Geophys. Res.: Oceans **122**(3): 2171-2182.

Anderson, E.J., Stow, C.A., Gronewold, A.D., Mason, L.A., McCormick, M.J., Qian, S.S., Ruberg, S.A., Beadle, K., Constant, S.A., and Hawley, N. 2021. Seasonal overturn and stratification changes drive deep-water warming in one of Earth's largest lakes. Nat. Commun. **12**(1): 1-9.

Beletsky, D., and Schwab, D. 2001. Modeling circulation and thermal structure in Lake Michigan: Annual cycle and interannual variability. J. Geophys. Res. **106**(C9): 19745-19771.

Beletsky, D., Mason, D.M., Schwab, D.J., Rutherford, E.S., Janssen, J., Clapp, D.F., and Dettmers, J.M. 2007. Biophysical model of larval yellow perch advection and settlement in Lake Michigan. J. Great Lakes Res. **33**(4): 842-866.

Beletsky, D., Beletsky, R., Rutherford, E.S., Sieracki, J.L., Bossenbroek, J.M., Chadderton, W.L., Wittmann, M.E., Annis, G.M., and Lodge, D.M. 2017. Predicting spread of aquatic invasive species by lake currents. J. Great Lakes Res. **43**(3): 14-32.

Benjamin, S.G., Weygandt, S.S., Brown, J.M., Hu, M., Alexander, C.R., Smirnova, T.G., Olson, J.B., James, E.P., Dowell, D.C., and Grell, G.A. 2016. A North American hourly assimilation and model forecast cycle: The Rapid Refresh. Mon. weather rev. **144**(4): 1669-1694.

Brodnik, R.M., Fraker, M.E., Anderson, E.J., Carreon-Martinez, L., DeVanna, K.M., Heath, D.D., Reichert, J.M., Roseman, E.F., and Ludsin, S.A. 2016. Larval dispersal underlies demographically important intersystem connectivity in a Great Lakes yellow perch (Perca flavescens) population. Can. J. Fish. Aquat. Sci. **73**(3): 416-426.

Bunnell, D.B., Warner, D.M., Madenjian, C.P., Turschak, B., Armenio, P., and Desorcie, T. 2020. Status and Trends of Pelagic and Benthic Prey Fish Populations in Lake Michigan, 20191, 2. Great Lake Fisheries Commission.

Bunnell, D.B., Barbiero, R.P., Ludsin, S.A., Madenjian, C.P., Warren, G.J., Dolan, D.M., Brenden, T.O., Briland, R., Gorman, O.T., and He, J.X. 2014. Changing ecosystem dynamics in the Laurentian Great Lakes: bottom-up and top-down regulation. BioScience **64**(1): 26-39.

Bunnell, D.B., Carrick, H.J., Madenjian, C.P., Rutherford, E.S., Vanderploeg, H.A., Barbiero, R.P., Hinchey-Malloy, E., Pothoven, S.A., Riseng, C.M., and Claramunt, R.M. 2018. Are changes in lower trophic levels limiting prey-fish biomass and production in Lake Michigan? Great Lakes Fishery Commission.

Chapra, S.C., and Dolan, D.M. 2012. Great Lakes total phosphorus revisited: 2. Mass balance modeling. J. Great Lakes Res. **38**(4): 741–754.

Chen, C., Liu, H., and Beardsley, R.C. 2003. An unstructured grid, finite-volume, three-dimensional, primitive equations ocean model: application to coastal ocean and estuaries. J. Atmos. Oceanic Technol. **20**(1): 159-186.

Choi, J., Troy, C., Hawley, N., McCormick, M., and Wells, M. 2020. Lateral dispersion of dye and drifters in the center of a very large lake. Limnol. Oceanogr. **65**(2): 336-348.

Choi, J.M., Troy, C.D., and Hawley, N. 2015. Shear dispersion from near‐inertial internal P oincaré waves in large lakes. Limnol. Oceanogr. **60**(6): 2222-2235.

Churchill, J.H., Runge, J., and Chen, C. 2011. Processes controlling retention of spring‐spawned Atlantic cod (Gadus morhua) in the western Gulf of Maine and their relationship to an index of recruitment success. Fish. Oceanogr. **20**(1): 32-46.

Clark Jr, R.D., Bence, J.R., Claramunt, R.M., Clevenger, J.A., Kornis, M.S., Bronte, C.R., Madenjian, C.P., and Roseman, E.F. 2017. Changes in movements of Chinook Salmon between Lakes Huron and Michigan after Alewife population collapse. North American Journal of Fisheries Management **37**(6): 1311-1331.

Csanady, G. 1975. Hydrodynamics of large lakes. Annual Review of Fluid Mechanics **7**(1): 357-386.

Davis, R.E. 1985. Drifter observations of coastal surface currents during CODE: The method and descriptive view. J. Geophys. Res.: Oceans **90**(C3): 4741-4755.

De Brauwere, A., De Brye, B., Servais, P., Passerat, J., and Deleersnijder, E. 2011. Modelling Escherichia coli concentrations in the tidal Scheldt river and estuary. Water Research **45**(9): 2724-2738.

Desai, A.R., Austin, J.A., Bennington, V., and McKinley, G.A. 2009. Stronger winds over a large lake in response to weakening air-to-lake temperature gradient. Nature Geoscience **2**(12): 855-858.

Dettmers, J.M., Goddard, C.I., and Smith, K.D. 2012. Management of alewife using Pacific salmon in the Great Lakes: whether to manage for economics or the ecosystem? Fisheries **37**(11): 495-501.

Dettmers, J.M., Janssen, J., Pientka, B., Fulford, R.S., and Jude, D.J. 2005. Evidence across multiple scales for offshore transport of yellow perch (Perca flavescens) larvae in Lake Michigan. Can. J. Fish. Aquat. Sci. **62**(12): 2683-2693.

Dunlop, E.S., and Riley, S.C. 2013. The contribution of cold winter temperatures to the 2003 alewife population collapse in Lake Huron. J. Great Lakes Res. **39**(4): 682-689.

Eggold, B., Gorenflo, T., Authority, C.-O.R., Price, J., Santucci, V., and Wesley, J. 2018. Lake Michigan Salmonine Stocking Strategy. Great Lakes Fishery Commission.

Eppehimer, D.E., Bunnell, D.B., Armenio, P.M., Warner, D.M., Eaton, L.A., Wells, D.J., and Rutherford, E.S. 2019. Densities, diets, and growth rates of larval alewife and bloater in a changing Lake Michigan ecosystem. Trans. Am. Fish. Soc. **148**(4): 755-770.

Essig, R.J., and Cole, C.F. 1986. Methods of estimating larval fish mortality from daily increments in otoliths. Trans. Am. Fish. Soc. **115**(1): 34-40.

Foley, C., and Collingsworth, P. 2018. Cooperative Science and Monitoring Initiative (CSMI) Lake Michigan 2015 Report. Illinois-Indiana Sea Grant, IISG18-HCE-RLA-013, https://repository.library.noaa.gov/view/noaa/37880/noaa_37880_DS1.pdf.

Goodyear, C.D. 1982. Atlas of the spawning and nursery areas of Great Lakes fishes. U.S. Fish and Wildlife Service, Washington D.C. FWS/OBS-82/52.

He, J.X., Bence, J.R., Madenjian, C.P., Pothoven, S.A., Dobiesz, N.E., Fielder, D.G., Johnson, J.E., Ebener, M.P., Cottrill, R.A., and Mohr, L.C. 2014. Coupling age-structured stock assessment and fish bioenergetics models: a system of time-varying models for quantifying piscivory patterns during the rapid trophic shift in the main basin of Lake Huron. Can. J. Fish. Aquat. Sci. **72**(1): 7-23.

Heufelder, G.R., Jude, D.J., and Tesar, F.J. 1982. Effects of upwelling on local abundance and distribution of larval alewife (Alosa pseudoharengus) in eastern Lake Michigan. Can. J. Fish. Aquat. Sci. **39**(11): 1531-1537.

Höök, T.O., Rutherford, E.S., Mason, D.M., and Carter, G.S. 2007. Hatch dates, growth, survival, and overwinter mortality of age-0 alewives in Lake Michigan: implications for habitat-specific recruitment success. Trans. Am. Fish. Soc. **136**(5): 1298-1312.

Höök, T.O., McCormick, M.J., Rutherford, E.S., Mason, D.M., and Carter, G.S. 2006. Short-term water mass movements in Lake Michigan: implications for larval fish transport. J. Great Lakes Res. **32**(4): 728-737.

Hunter, J., Craig, P., and Phillips, H. 1993. On the use of random walk models with spatially variable diffusivity. Journal of Computational Physics **106**(2): 366-376.

Huret, M., Runge, J., Chen, C., Cowles, G., Xu, Q., and Pringle, J. 2007. Dispersal modeling of fish early life stages: sensitivity with application to Atlantic cod in the western Gulf of Maine. Marine Ecol.: Prog. Ser. **347**: 261-274.

James, E.P., Benjamin, S.G., and Marquis, M. 2018. Offshore wind speed estimates from a high‐resolution rapidly updating numerical weather prediction model forecast dataset. Wind Energy **21**(4): 264-284.

Johnson, J.E., DeWitt, S.P., and Gonder, D.J. 2010. Mass-marking reveals emerging self regulation of the Chinook salmon population in Lake Huron. North American Journal of Fisheries Management **30**(2): 518-529.

Kao, Y.-C., Adlerstein, S.A., and Rutherford, E.S. 2016. Assessment of top-down and bottom-up controls on the collapse of alewives (*Alosa pseudoharengus*) in Lake Huron. Ecosystems. doi:10.1007/s10021-016-9969-y.

Kelley, J.G.W., Chen, Y., Anderson, E.J., Lang, G.A., and Peng, M. 2020. Upgrade of NOS Lake Michigan and Lake Huron operational forecast systems to FVCOM : model development and hindcast skill assessment [Technical Memorandum]. doi:https://doi.org/10.25923/mmyb-qh56.

Klumb, R.A., Rudstam, L.G., and Mills, E.L. 2003. Comparison of alewife young-of-the-year and adult respiration and swimming speed bioenergetics model parameters: implications of extrapolation. Trans. Am. Fish. Soc. **132**(6): 1089-1103.

Kraemer, B.M., Anneville, O., Chandra, S., Dix, M., Kuusisto, E., Livingstone, D.M., Rimmer, A., Schladow, S.G., Silow, E., and Sitoki, L.M. 2015. Morphometry and average temperature affect lake stratification responses to climate change. Geophys. Res. Lett. **42**(12): 4981-4988.

LaBay, S.R., and Lauer, T.E. 2006. An evaluation of the accuracy of age estimation methods for southern Lake Michigan alewives. North American Journal of Fisheries Management **26**(3): 571-579.

Ludsin, S.A., DeVanna, K.M., and Smith, R.E. 2014. Physical–biological coupling and the challenge of understanding fish recruitment in freshwater lakes. Can. J. Fish. Aquat. Sci. **71**(5): 775-794.

Madenjian, C., and Jude, D.J. 1985. Comparison of sleds versus plankton nets for sampling fish larvae and eggs. Hydrobiologia **124**(3): 275-281.

Mao, M., and Xia, M. 2020a. Monthly and episodic dynamics of summer circulation in Lake Michigan. J. Geophys. Res.: Oceans **125**(6): e2019JC015932.

Mao, M., and Xia, M. 2020b. Particle Dynamics in the Nearshore of Lake Michigan Revealed by an Observation‐Modeling System. J. Geophys. Res.: Oceans **125**(8): e2019JC015765.

Nash, R.D., and Geffen, A.J. 1991. Spatial and temporal changes in the offshore larval fish assemblage in southeastern Lake Michigan. J. Great Lakes Res. **17**(1): 25-32.

Norden, C.R. 1968. Morphology and food habits of the larval alewife, Alosa pseudoharengus (Wilson), in Lake Michigan. Trans. Am. Fish. Soc. **96**(4): 387-393. doi:10.1577/1548-8659(1967)96[387:AGAFOT]2.0.CO;2.

Peng, M., Zhang, A., Anderson, E.J., Lang, G.A., Kelley, J.G.W., and Chen, Y. 2019. Implementation of the Lakes Michigan and Huron Operational Forecast System (LMHOFS) and the Nowcast/Forecast Skill Assessment [Technical Report]. doi:https://doi.org/10.25923/cy7n-ja86.

Plattner, S., Mason, D.M., Leshkevich, G.A., Schwab, D.J., and Rutherford, E.S. 2006. Classifying and forecasting coastal upwellings in Lake Michigan using satellite derived temperature images and buoy data. J. Great Lakes Res. **32**(1): 63-76.

Pritt, J.J., Roseman, E.F., and O'Brien, T.P. 2014. Mechanisms driving recruitment variability in fish: comparisons between the Laurentian Great Lakes and marine systems. ICES Journal of Marine Science **71**(8): 2252-2267.

Rao, Y.R., and Schwab, D.J. 2007. Transport and mixing between the coastal and offshore waters in the Great Lakes: a review. J. Great Lakes Res. **33**(1): 202-218.

Riley, S.C., Roseman, E.F., Nichols, S.J., O'Brien, T.P., Kiley, C.S., and Schaeffer, J.S. 2008. Deepwater demersal fish community collapse in Lake Huron. T. Am. Fish. Soc. **137**(6): 1879-1890.

Röhrs, J., Christensen, K.H., Hole, L.R., Broström, G., Drivdal, M., and Sundby, S. 2012. Observation-based evaluation of surface wave effects on currents and trajectory forecasts. Ocean Dynamics **62**(10): 1519-1533.

Rowe, M.D., Obenour, D.R., Nalepa, T.F., Vanderploeg, H.A., Yousef, F., and Kerfoot, W.C. 2015. Mapping the spatial distribution of the biomass and filter‐feeding effect of invasive dreissenid mussels on the winter‐spring phytoplankton bloom in Lake Michigan. Freshwater Biol. **60**(11): 2270-2285.

Rowe, M.D., Anderson, E.J., Wynne, T.T., Stumpf, R.P., Fanslow, D.L., Kijanka, K., Vanderploeg, H.A., Strickler, J.R., and Davis, T.W. 2016. Vertical distribution of buoyant Microcystis blooms in a Lagrangian particle tracking model for short-term forecasts in Lake Erie. J. Geophys. Res.: Oceans ***121***. doi:10.1002/2016JC011720.

Stadig, M.H., Collingsworth, P.D., Lesht, B.M., and Höök, T.O. 2020. Spatially heterogeneous trends in nearshore and offshore chlorophyll a concentrations in lakes Michigan and Huron (1998–2013). Freshwater Biol. **65**(3): 366-378.

Thupaki, P., Phanikumar, M.S., and Whitman, R.L. 2013. Solute dispersion in the coastal boundary layer of southern Lake Michigan. J. Geophys. Res.: Oceans **118**(3): 1606-1617.

Vanderploeg, H.A., Liebig, J.R., Nalepa, T.F., Fahnenstiel, G.L., and Pothoven, S.A. 2010. *Dreissena* and the disappearance of the spring phytoplankton bloom in Lake Michigan. J. Great Lakes Res. **36**(S3): 50-59.

Webb, A., and Fox-Kemper, B. 2011. Wave spectral moments and Stokes drift estimation. Ocean Model. **40**(3-4): 273-288.

Weber, M.J., Dettmers, J.M., and Wahl, D.H. 2011. Growth and survival of age-0 yellow perch across habitats in southwestern Lake Michigan: early life history in a large freshwater environment. T. Am. Fish. Soc. **140**(5): 1172-1185.

Weber, M.J., Ruebush, B.C., Creque, S.M., Redman, R.A., Czesny, S.J., Wahl, D.H., and Dettmers, J.M. 2015. Early life history of alewife *Alosa pseudoharengus* in southwestern Lake Michigan. J. Great Lakes Res.

Withers, J.L., Sesterhenn, T. M., Foley, C. J., Troy, C. D., Höök, T. O. . 2015. Diets and growth potential of early stage larval yellow perch and alewife in a nearshore region of southeastern Lake Michigan. J. Great Lakes Res. **3**(41): 197-209.

Xue, P., Pal, J.S., Ye, X., Lenters, J.D., Huang, C., and Chu, P.Y. 2017. Improving the simulation of large lakes in regional climate modeling: Two-way lake–atmosphere coupling with a 3D hydrodynamic model of the Great Lakes. Journal of Climate **30**(5): 1605-1627.

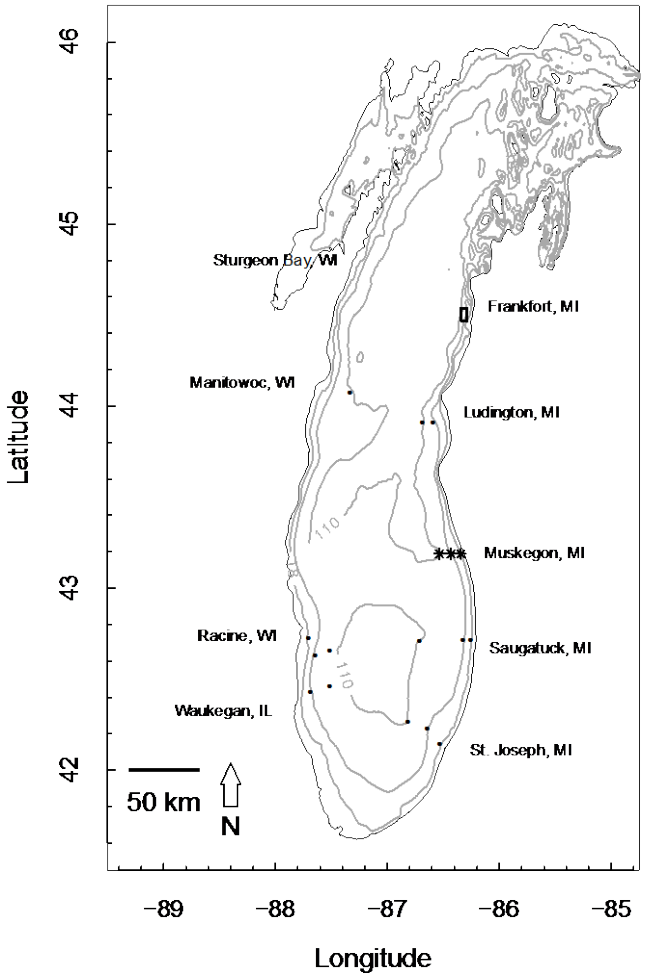

Figure 1. Map of Lake Michigan, with bathymetry contours (15, 45, and 110-m), and port cities in the US States of Michigan (MI), Wisconsin (WI), and Illinois (IL). Locations of larval alewife collections (solid circles), and drifter deployment stations located at 15, 45, and 110-m depth offshore of Muskegon (asterisks; M15, M45, M110) are indicated. Stations offshore of Sturgeon Bay and Frankfort were sampled, but no larval alewife were collected.

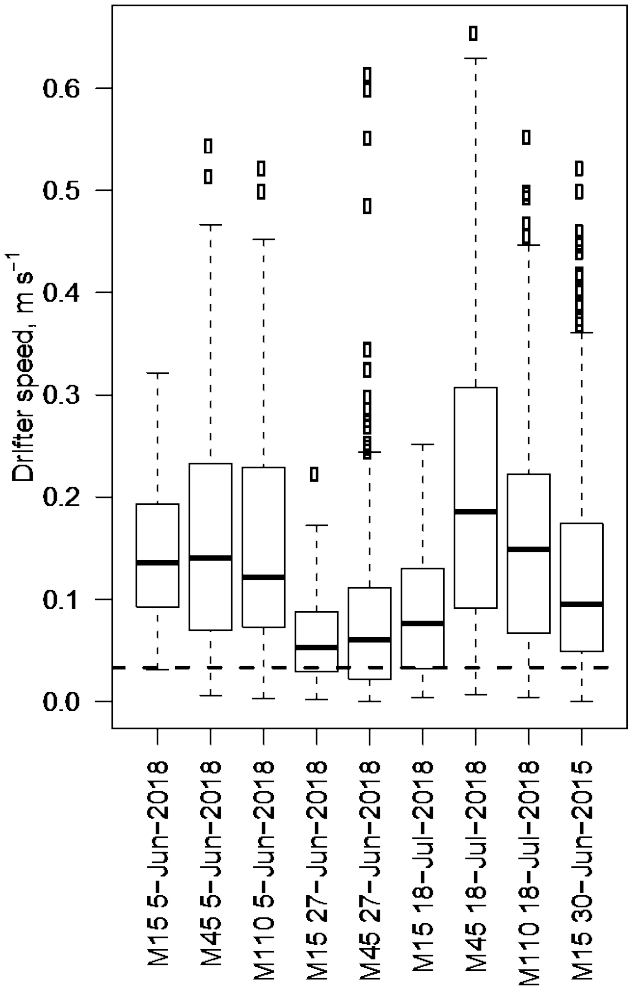

Figure 2. Drifting speeds recorded by satellite-tracked drifting buoys deployed at stations offshore of Muskegon, MI (Figure 1), in June and July of 2015 and 2018. The horizontal dashed line indicates an estimate of larval alewife swimming speed (see Discussion). Box plots indicate the median and interquartile range, with whiskers extending to the most extreme value within 1.5 times the interquartile range, and circles indicating values outside the range of the whiskers.

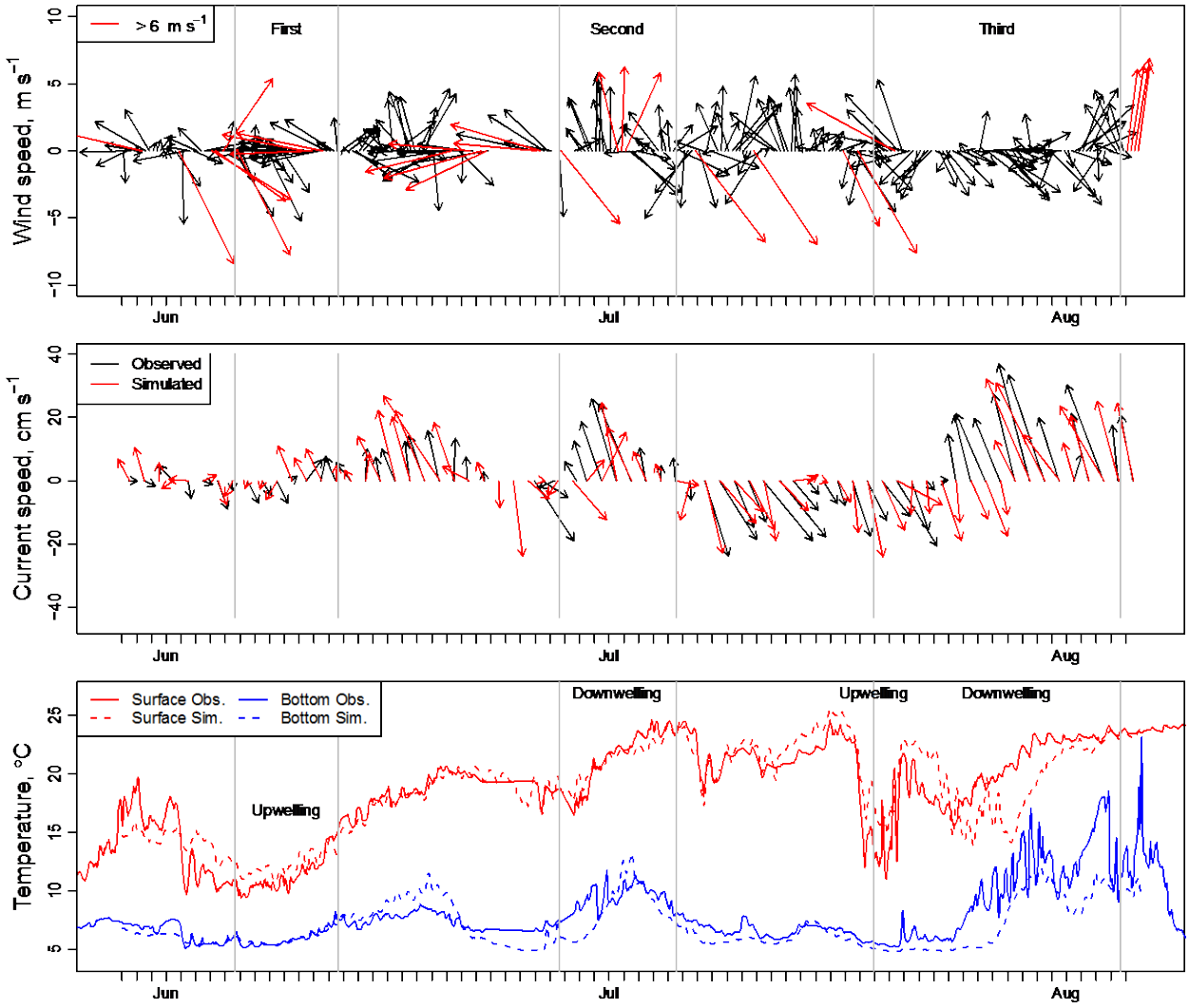

Figure 3. Observed wind, currents, surface and bottom temperature at the Muskegon M15 station (Figure 1) during the first, second, and third 2018 drifter deployments, with periods of upwelling and downwelling indicated. Wind and currents are averaged over six hours. Wind vector arrows highlighted in red were > 6 m s^{-1} speed. FVCOM model simulated currents and temperatures are plotted along with observations.

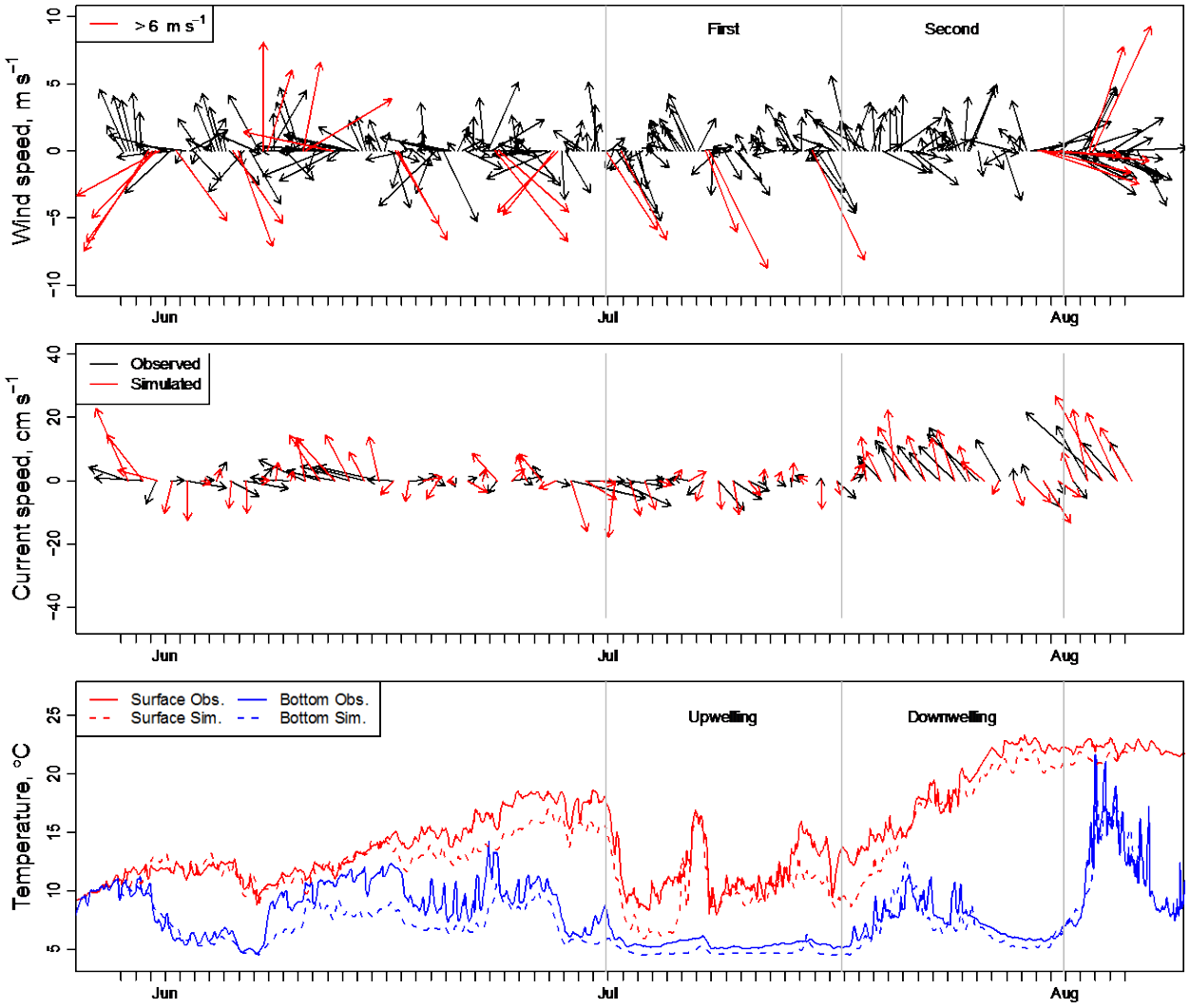

Figure 4: Observed wind, currents, surface and bottom temperature at the M15 station (Figure 1) during the first, second, and third 2015 drifter deployments. Symbols are explained in Fig. 3 caption.

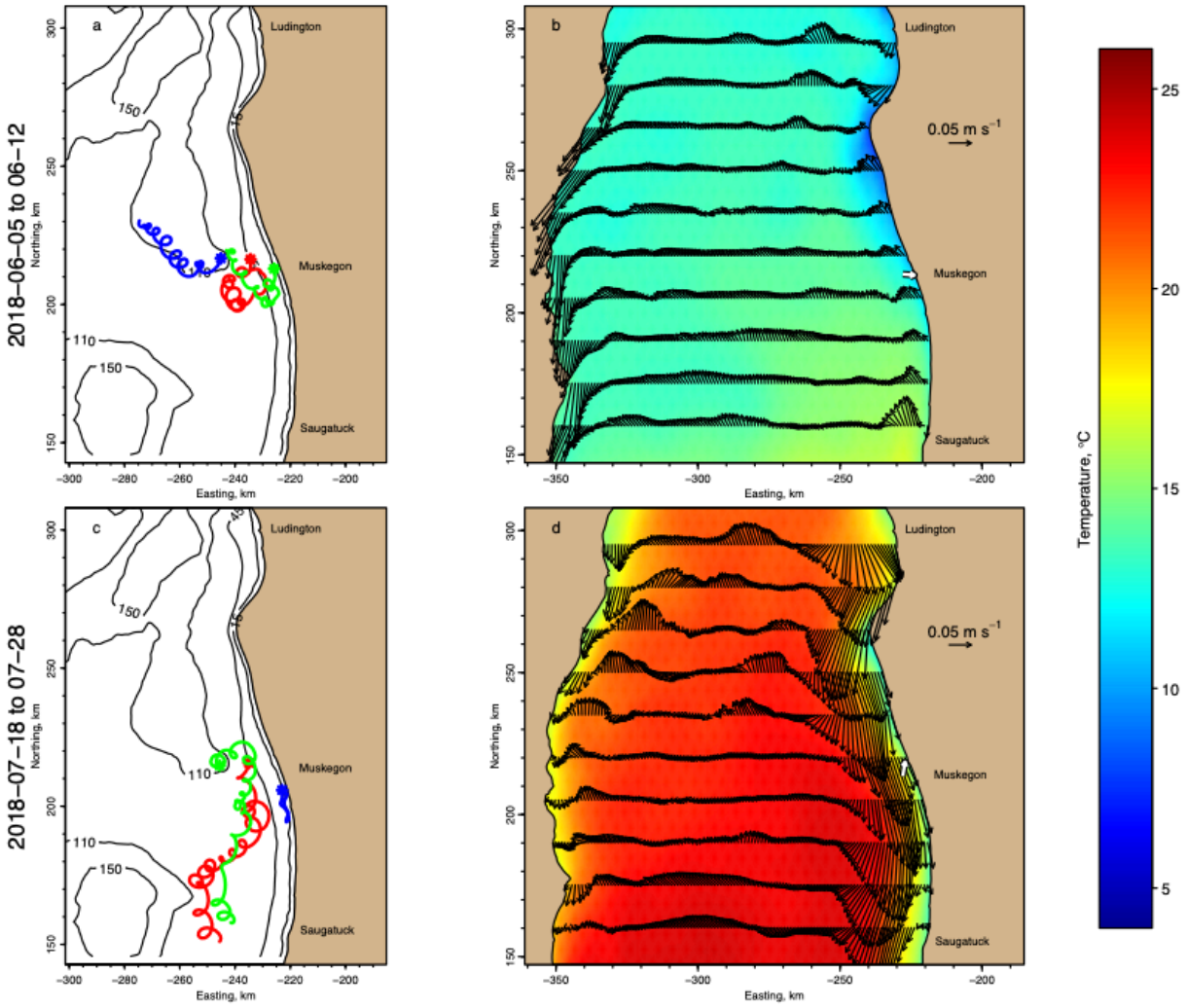

Figure 5. 2018 satellite-tracked drifter buoy trajectories, model currents and surface temperature for upwelling periods (Figure 3) offshore of Muskegon. The observed surface current vector at the Muskegon ADCP averaged over the period is indicated by a white arrow with black outline. Model currents are plotted at 1km spacing in easting and 15km spacing in northing to visualize coastal currents.

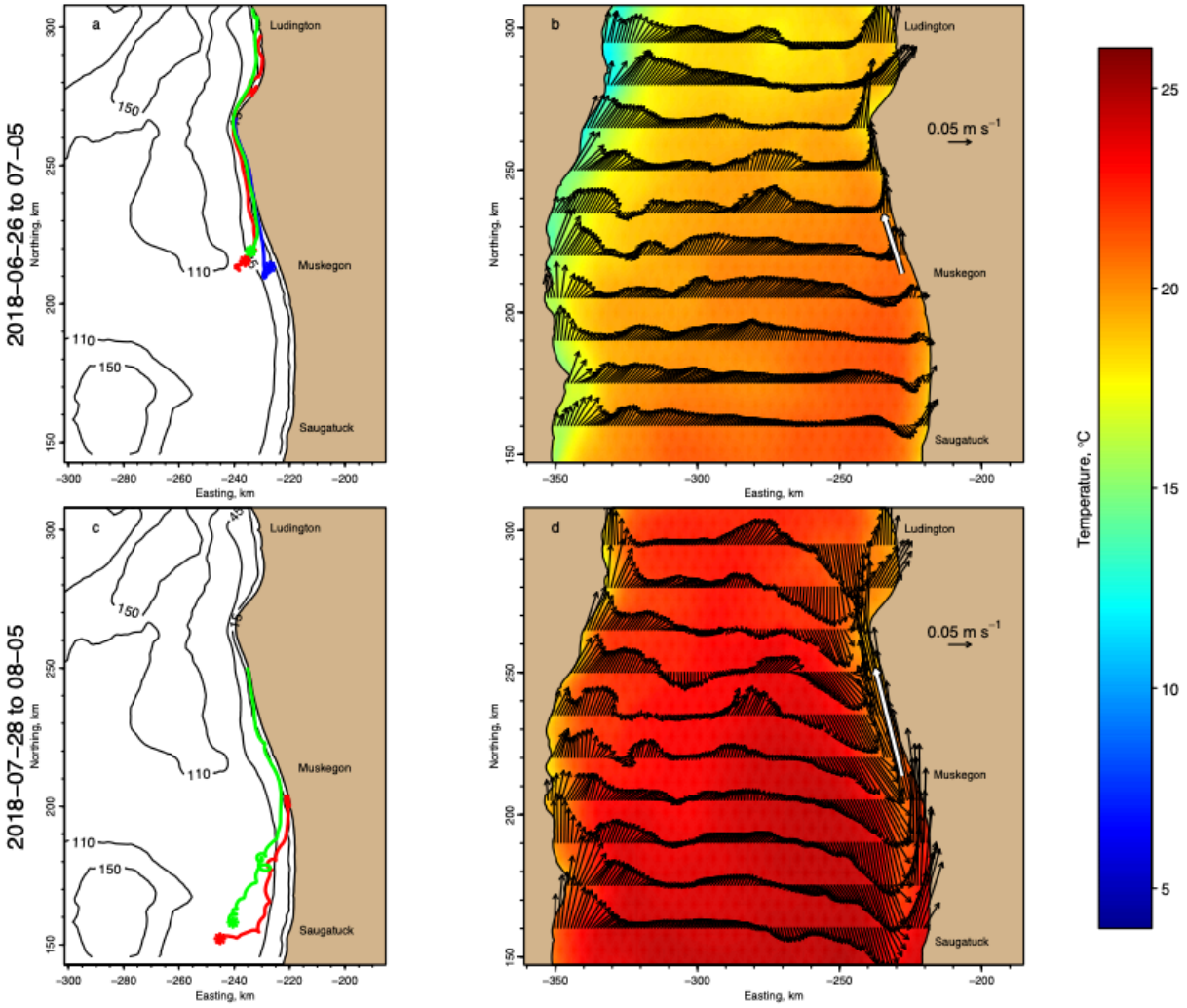

Figure 6. 2018 drifter trajectories, model currents and surface temperature for downwelling periods (Figure 3) offshore of Muskegon. Other symbols are explained in Figure 4.

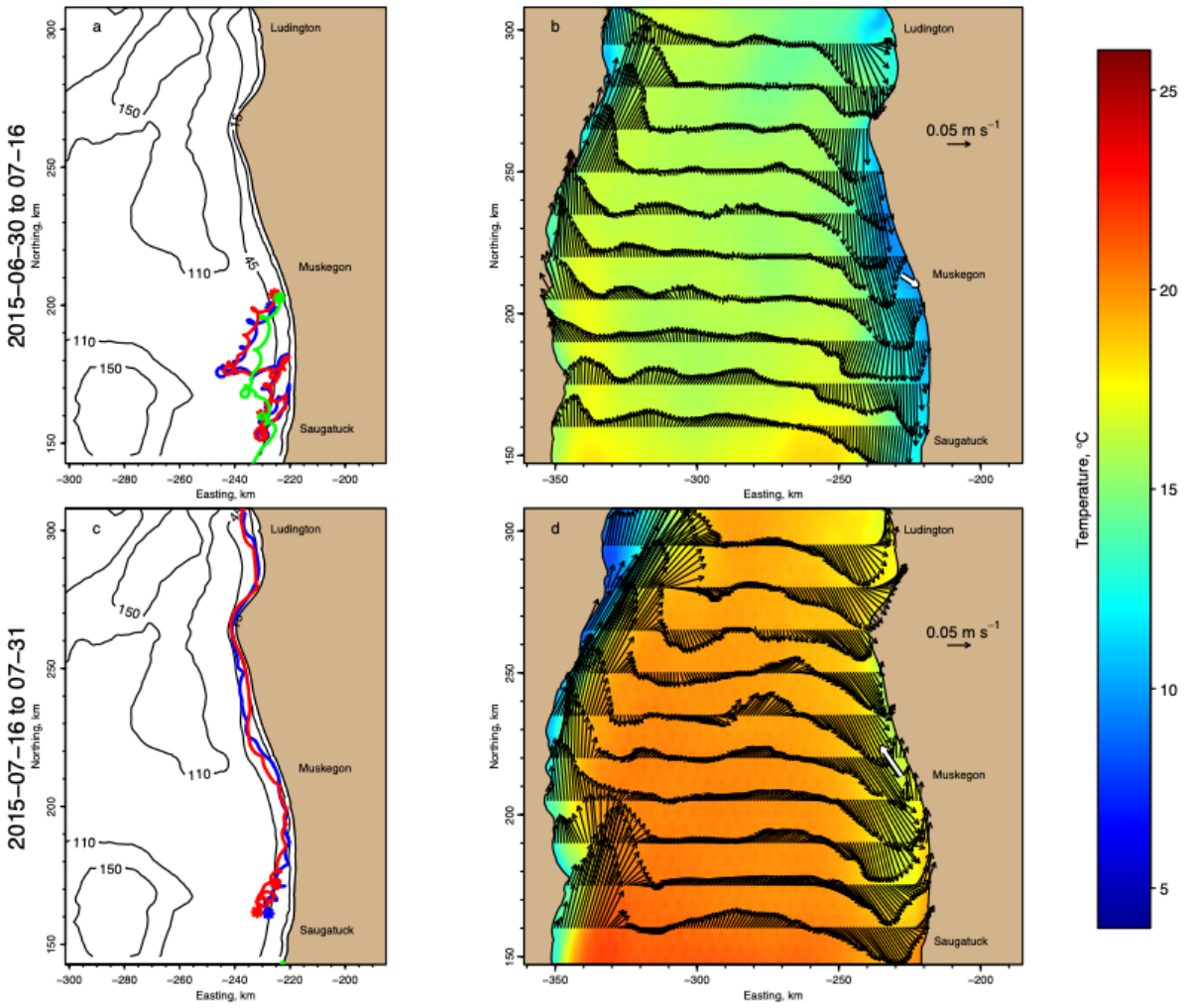

Figure 7. 2015 drifter trajectories, model currents and surface temperature, divided into periods of upwelling (a,b) and downwelling (c,d). Other symbols are explained in Figure 4.

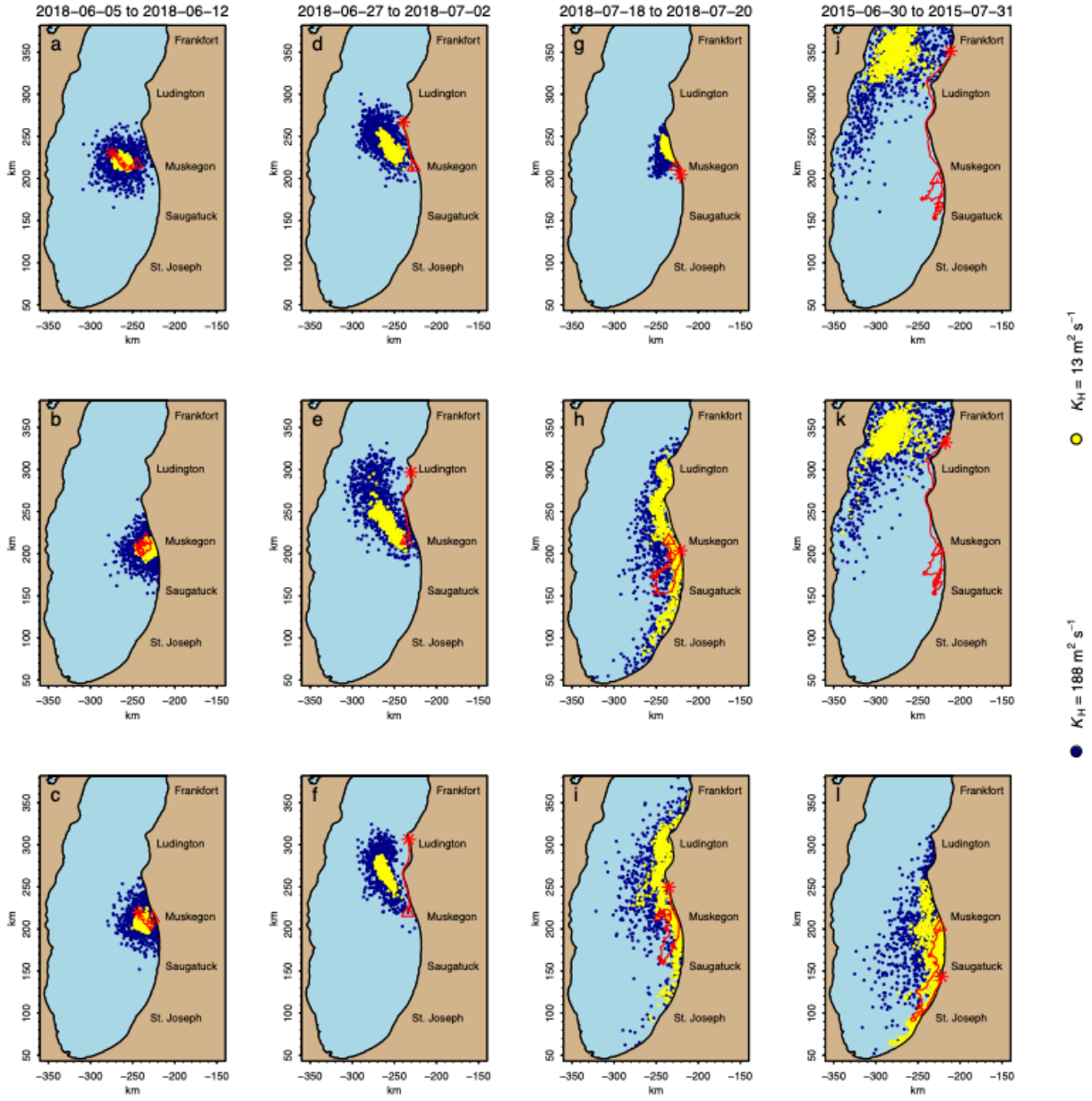

Figure 8. Prediction of the origin of satellite-tracked drifter buoys from their final position and drift duration using backward trajectory simulations. The model-predicted drifter origin is given as a spatial patch represented by colored points indicating two scenarios of horizontal diffusivity: $K_H = 13$ m^2 s^{-1} (yellow) and 188 m^2 s^{-1} (navy blue). The observed drifter origin, track, and final location are shown by a red triangle, solid line, and asterisk, respectively.

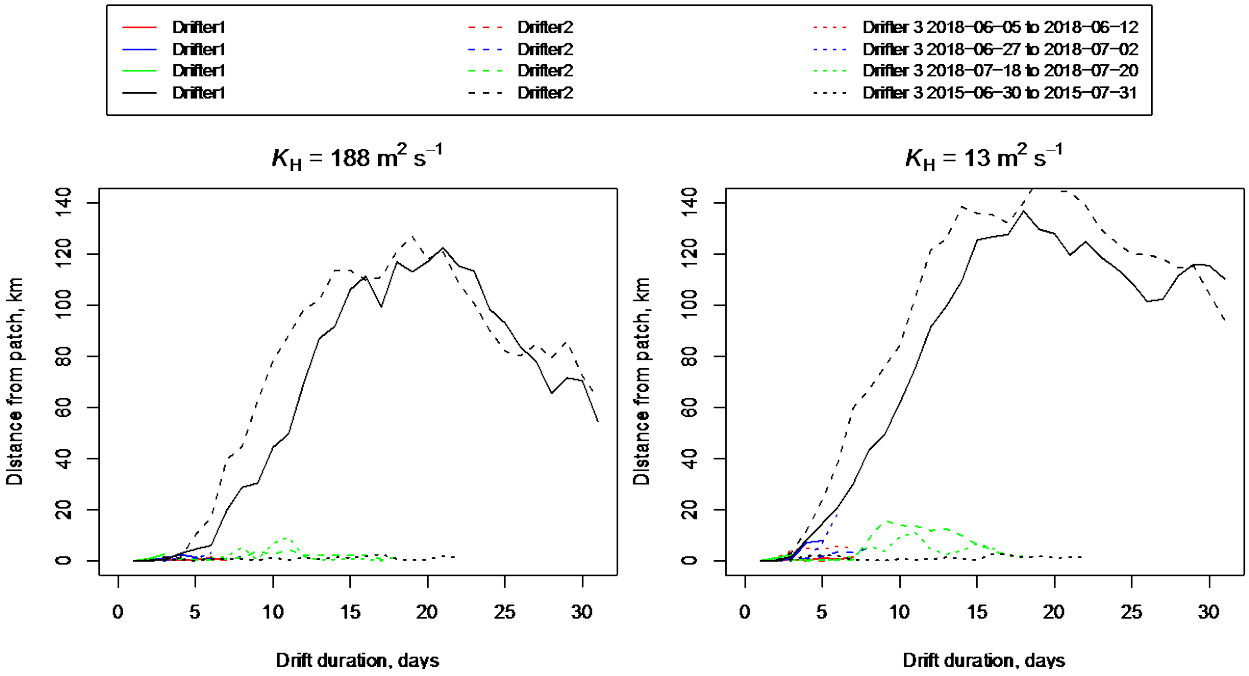

Figure 9. Model skill in predicting possible drifter buoy origins for the backward trajectory simulations in Figure 8, given as the minimum distance between the observed drifter position and the spatial patch of likely drifter origin locations (nearest Lagrangian particle). The two panels give results for the two scenarios of horizontal diffusivity (K_H = 13 m^2 s^{-1} and 188 m^2 s^{-1}). Line color indicates the deployment period, given in the legend, while each individual drifter within a deployment period is shown with a different line type (solid, dashed, dotted).

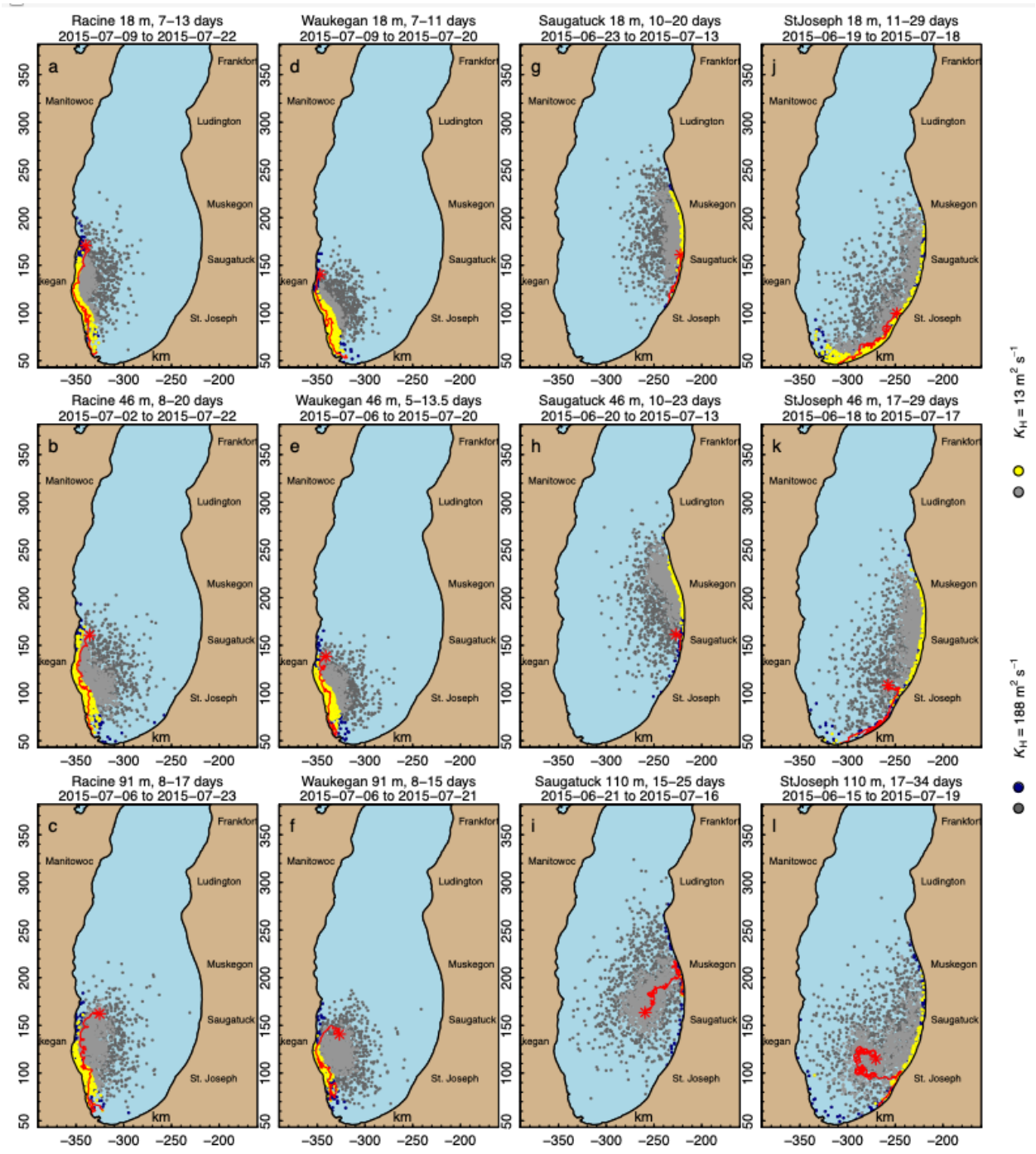

Figure 10. Predicted origins of alewife larvae in southern Lake Michigan using two scenarios of horizontal diffusivity, $K_H = 13$ m^2 s^{-1} (yellow) and 188 m^2 s^{-1} (navy blue), within a range of depths that were plausible for spawning (< 20 m bottom depth). Gray areas indicate estimated origin locations in deep water, not likely to be spawning areas. Backward trajectory

simulations began at the site of field collection (red asterisk) and ran for the duration of the oldest age larva collected in that sample, with the range of ages indicated above each panel. The red line illustrates one example from the ensemble of model backward trajectories, over the date range indicated above each panel.

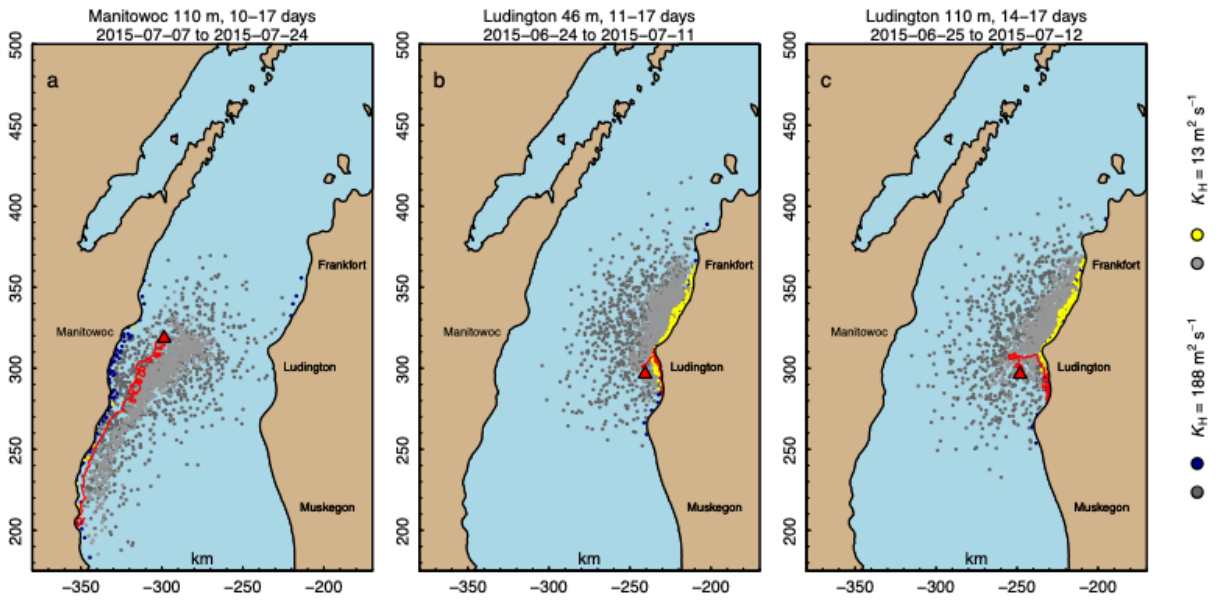

Figure 11. Predicted origins of alewife larvae in northern Lake Michigan using two scenarios of horizontal diffusivity, $K_H = 13$ m^2 s^{-1} (yellow) and 188 m^2 s^{-1} (navy blue), within a range of depths that were plausible for spawning (< 20 m bottom depth). Gray areas indicate estimated origin locations in deep water, not likely to be spawning areas. Backward trajectory simulations began at the site of field collection (red asterisk) and ran for the duration of the oldest age larva collected in that sample, with the range of ages indicated above each panel. The red line illustrates one example from the ensemble of model backward trajectories, over the date range indicated above each panel.

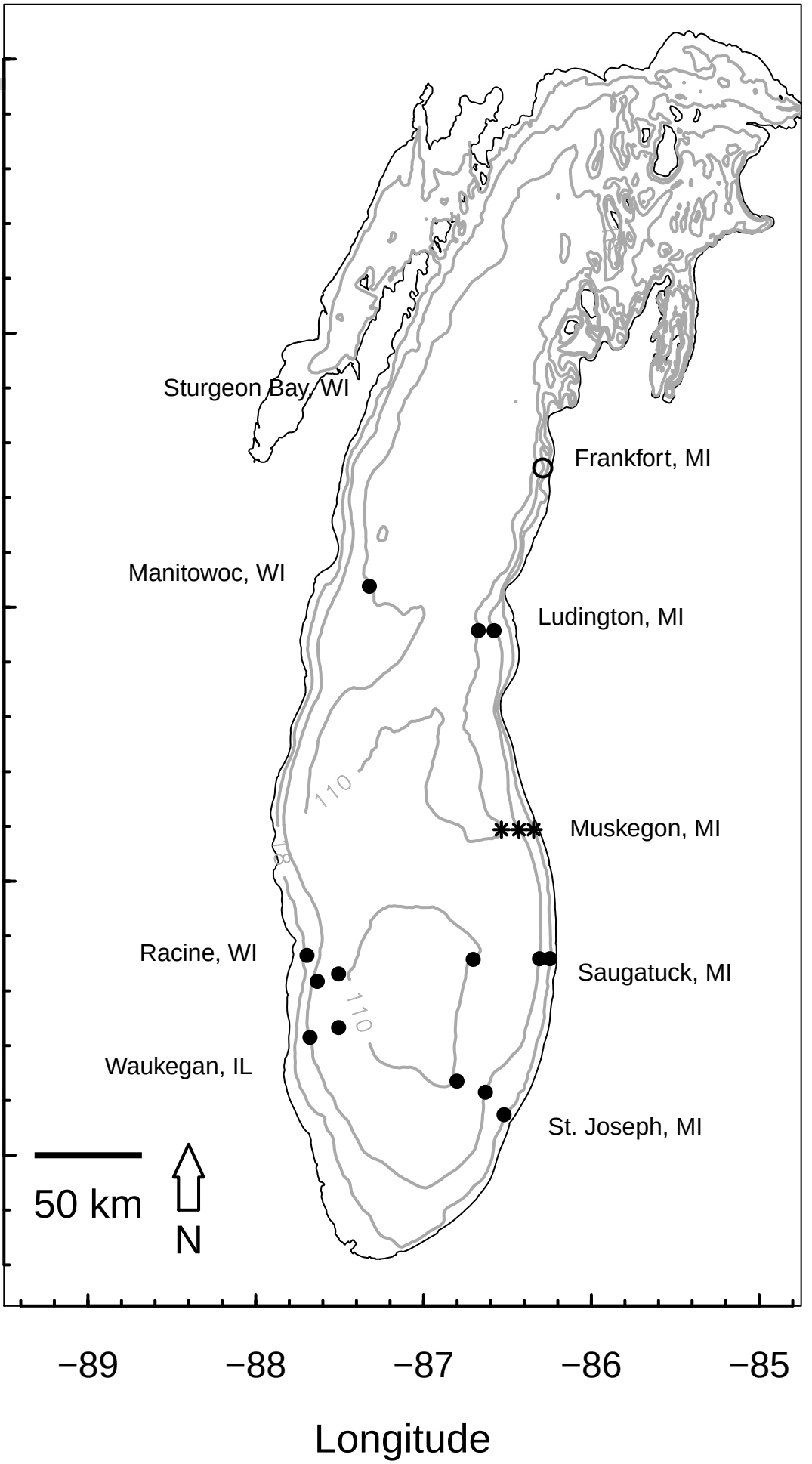

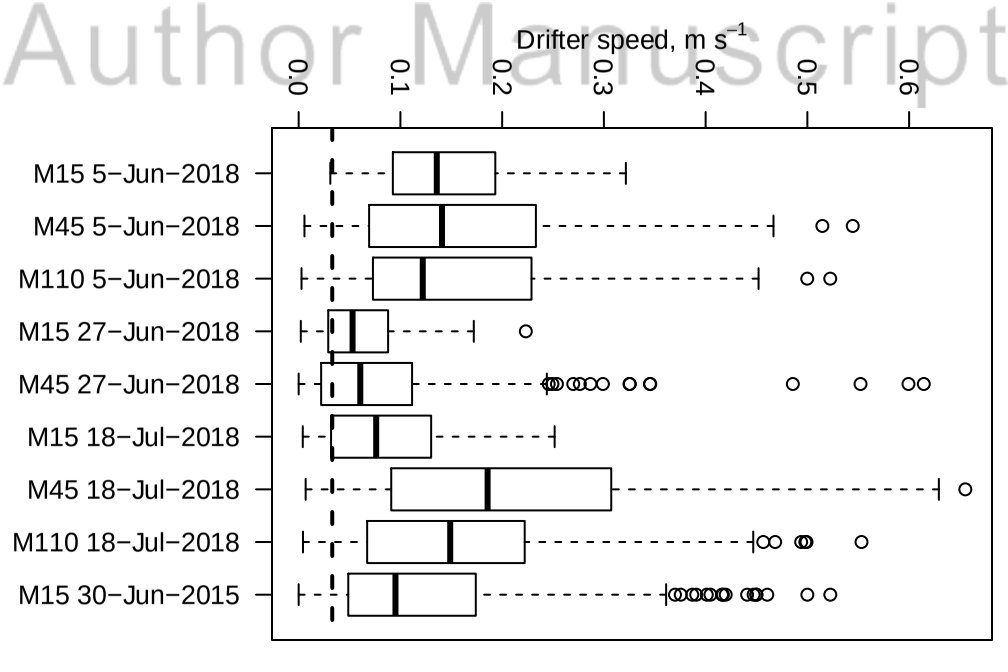

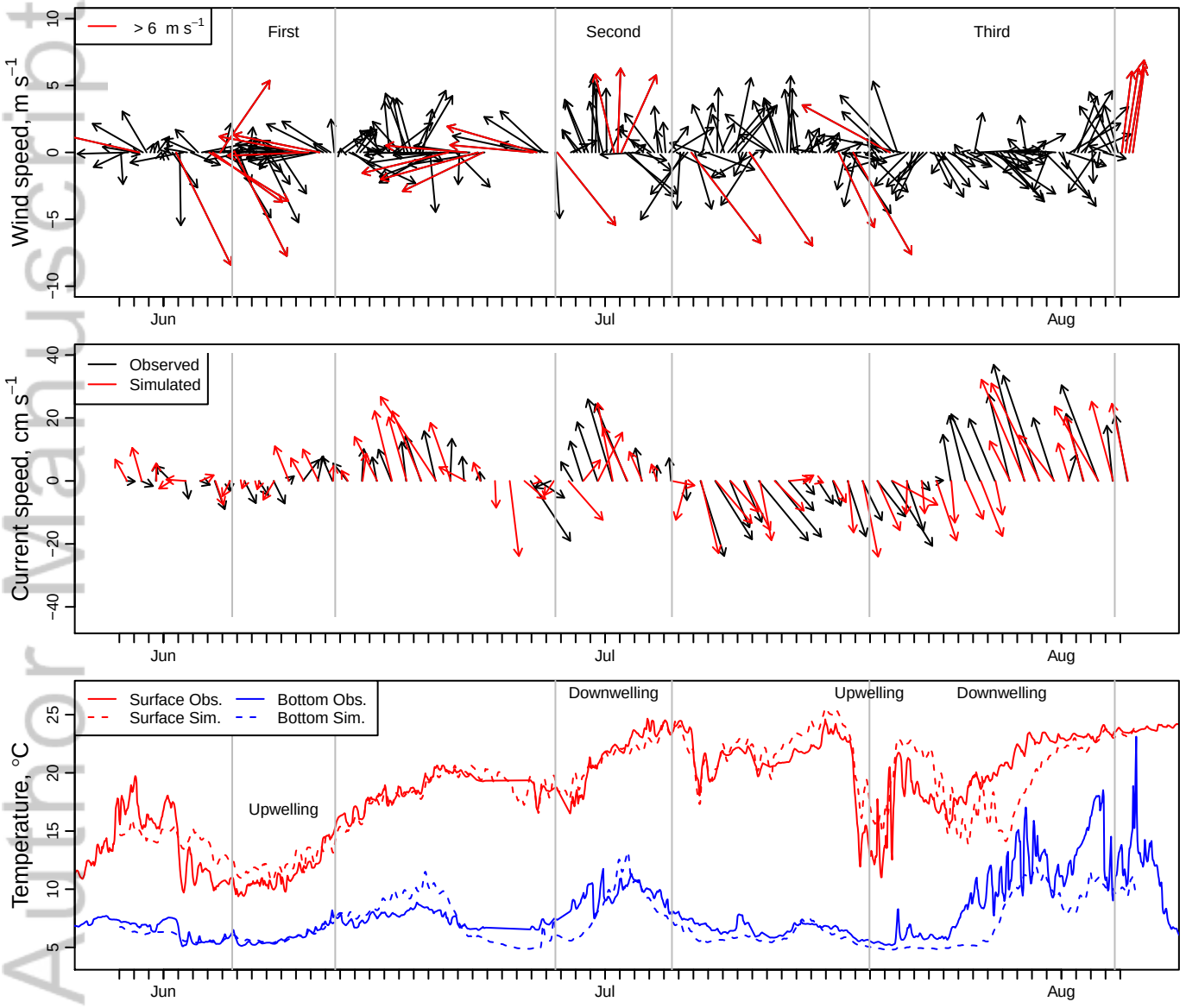
> 6 m s−1
First
Second
Third
Wind speed, m s−1
10
5
0
−5
−10
Jun
Jul
Aug
Observed
Simulated
Current speed, cm s−1
40
20
0
−20
−40
Jun
Jul
Aug
Surface Obs.
Surface Sim.
Bottom Obs.
Bottom Sim.
Downwelling
Upwelling
Upwelling
Downwelling
Temperature, °C
25
20
15
10
5
Jun
Jul
Aug

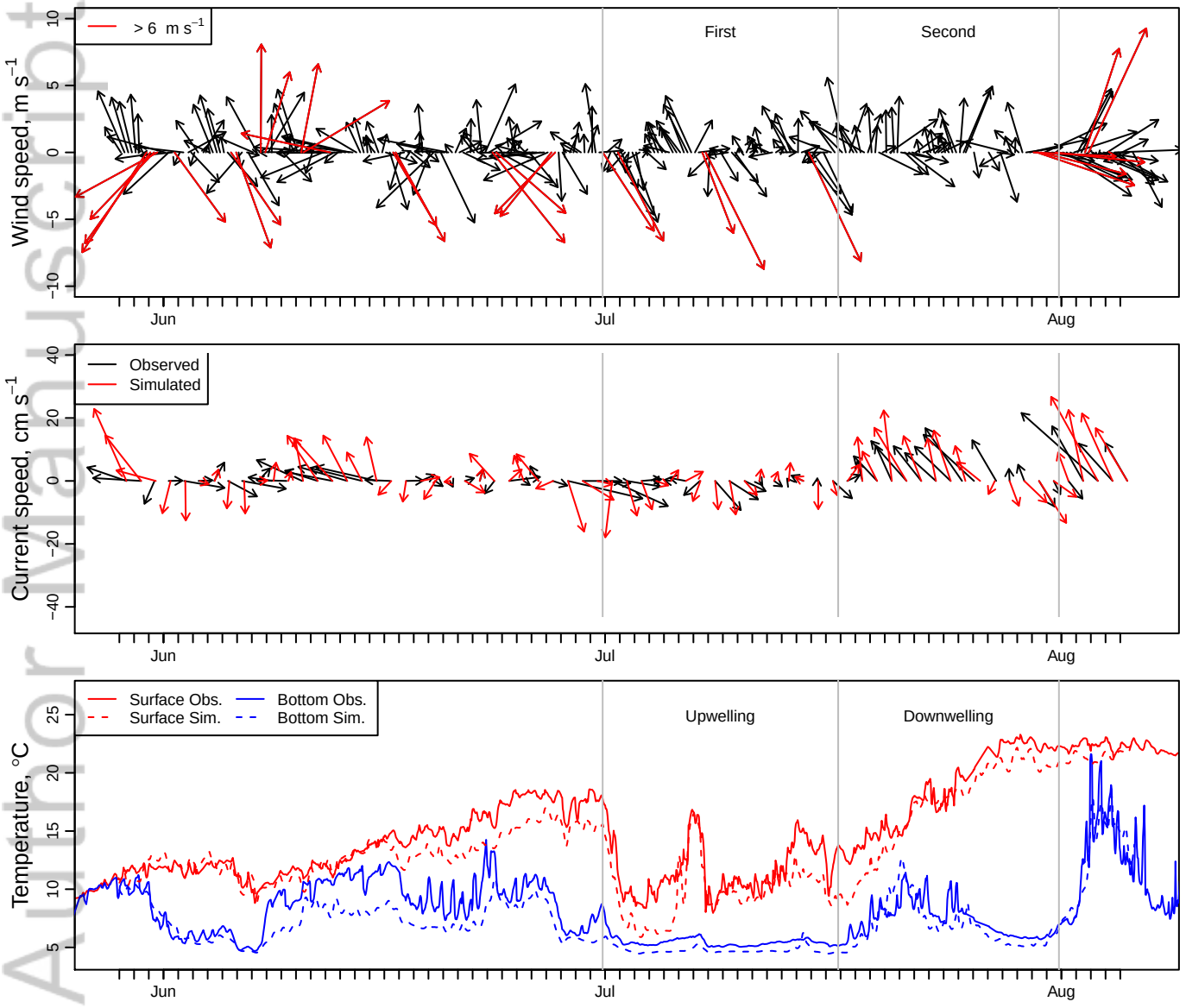
> 6 m s−1
First
Second
Wind speed, m s−1
10
5
0
−5
−10
Jun
Jul
Aug
Observed
Simulated
Current speed, cm s−1
40
20
0
−20
−40
Jun
Jul
Aug
Surface Obs.
Surface Sim.
Bottom Obs.
Bottom Sim.
Upwelling
Downwelling
Temperature, °C
25
20
15
10
5
Jun
Jul
Aug

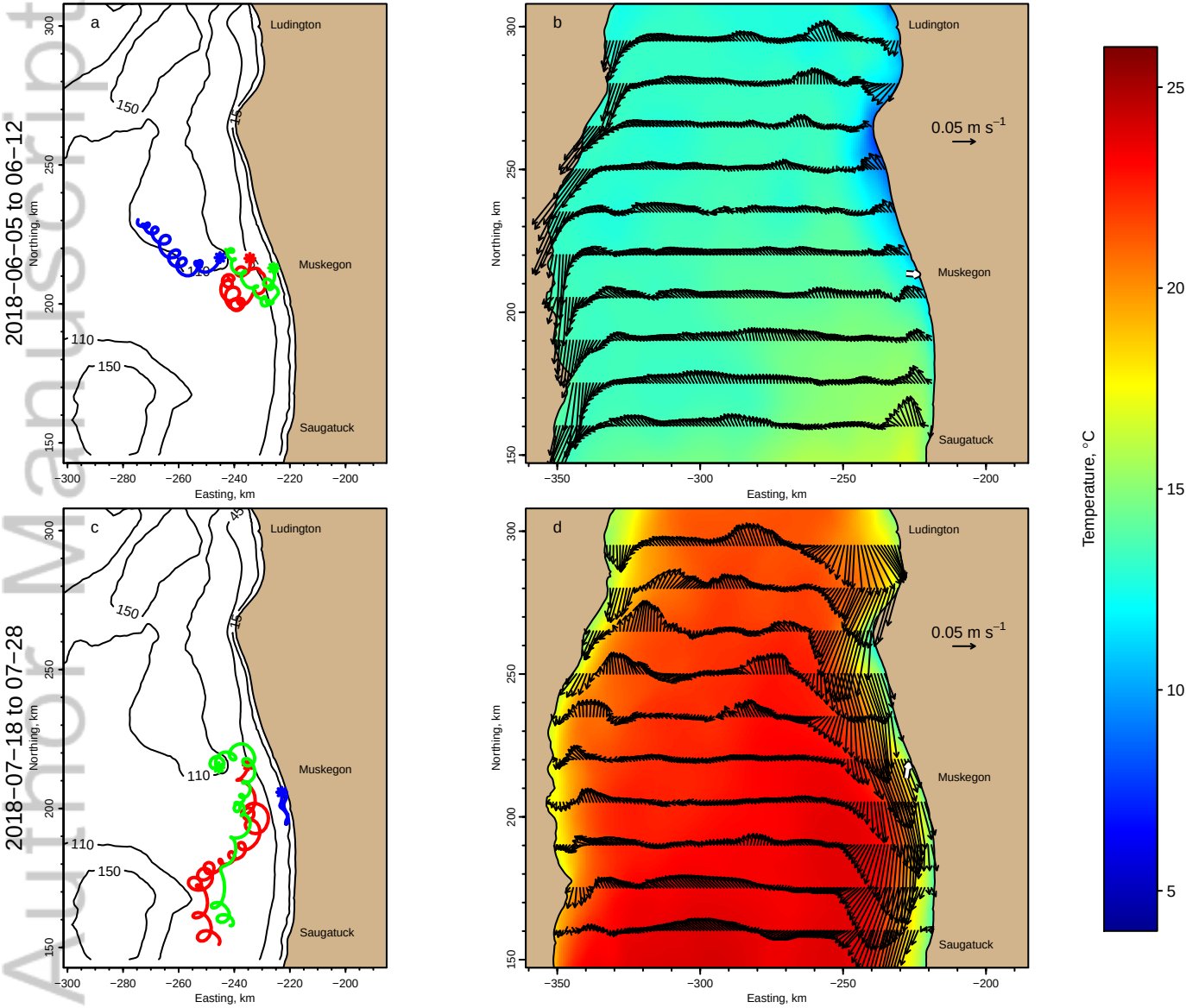

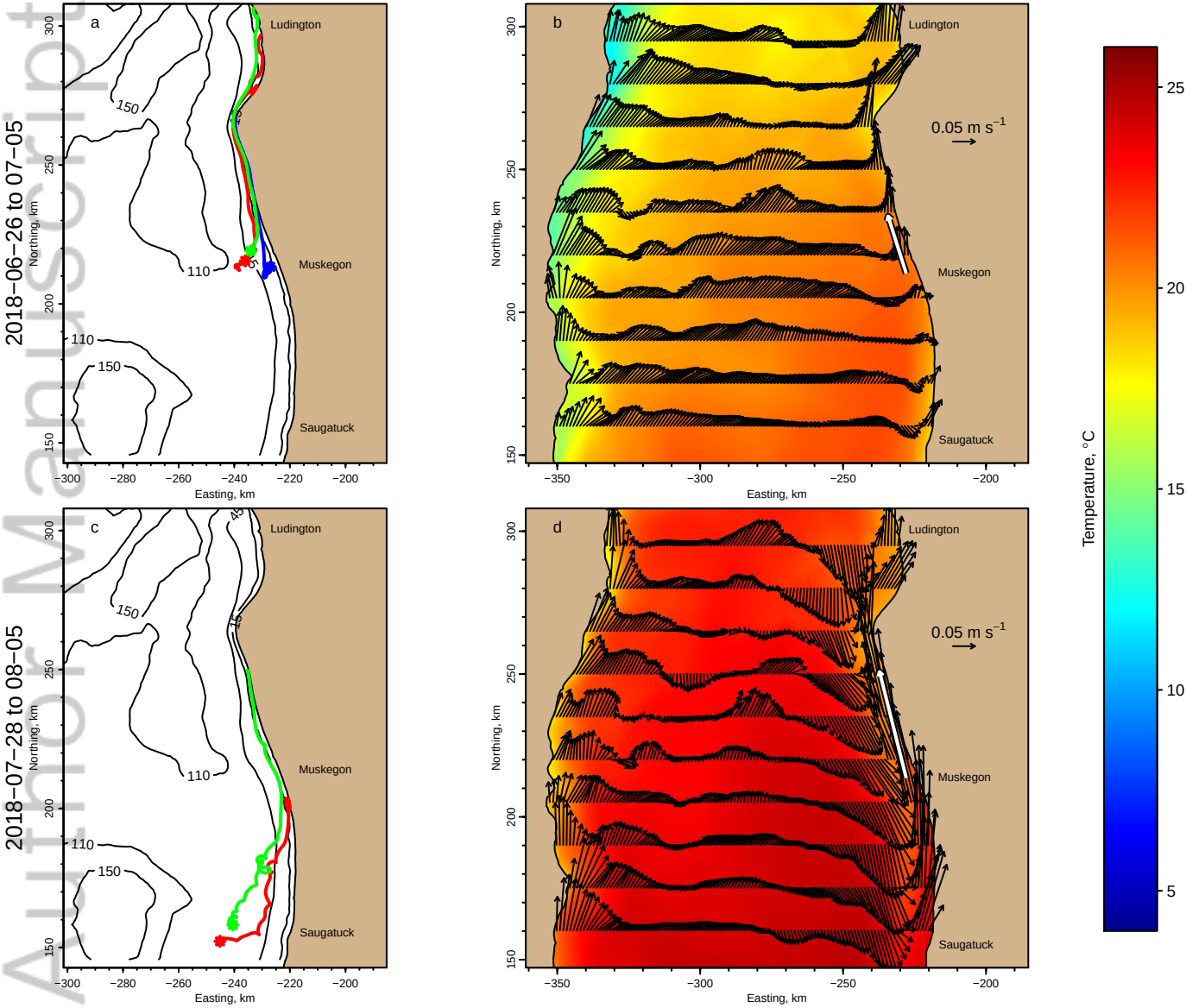
a
b
c
d
Ludington
Muskegon
Saugatuck
150
110
45
15
5
0.05 m s^{-1}
Northing, km
Easting, km
Temperature, °C
2018–06–26 to 07–05
2018–07–28 to 08–05
Author Manuscript

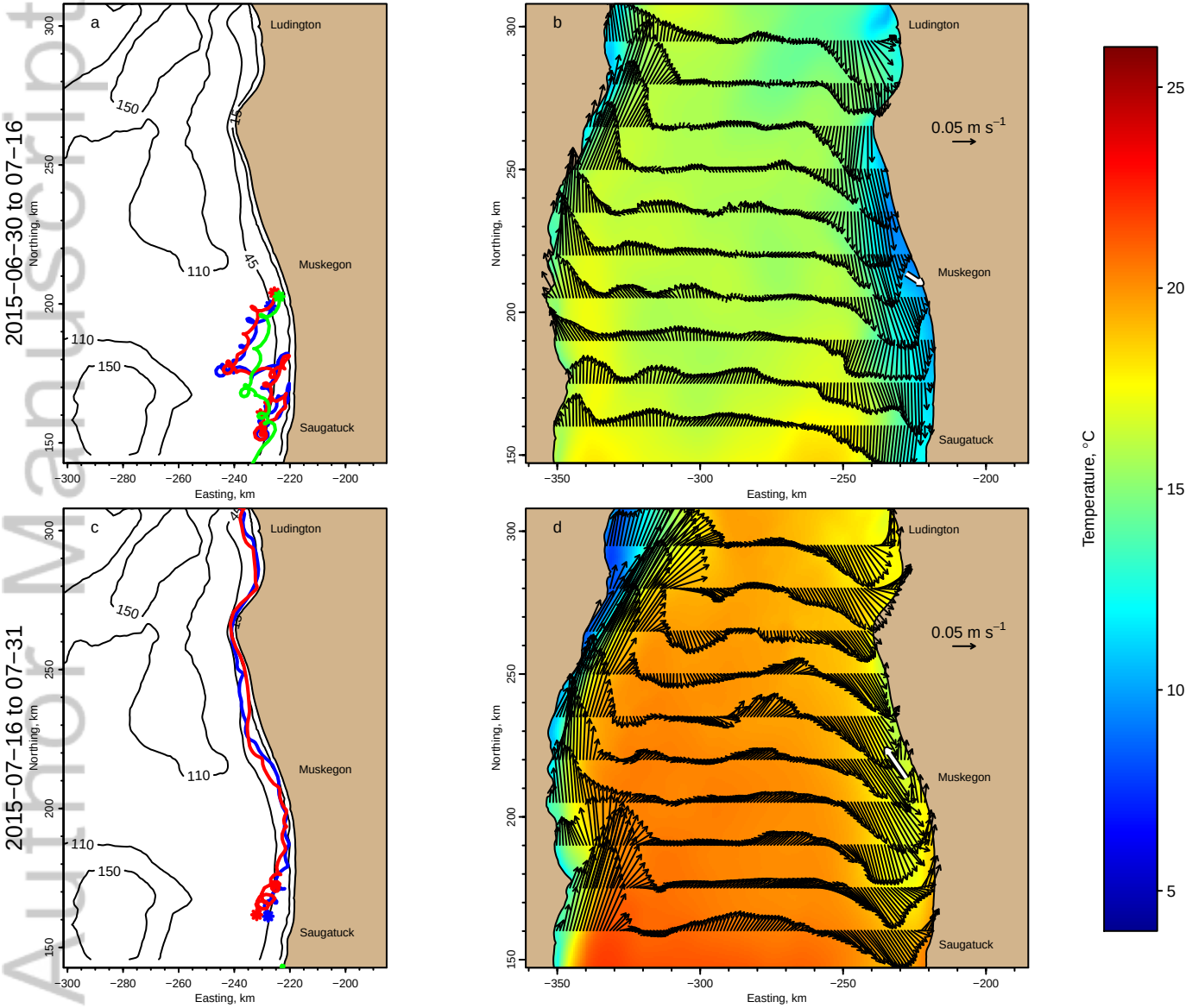
a
b
c
d
Ludington
Muskegon
Saugatuck
150
110
45
0.05 m s^{-1}
Northing, km
Easting, km
Temperature, °C
2015–06–30 to 07–16
2015–07–16 to 07–31
Author Manuscript

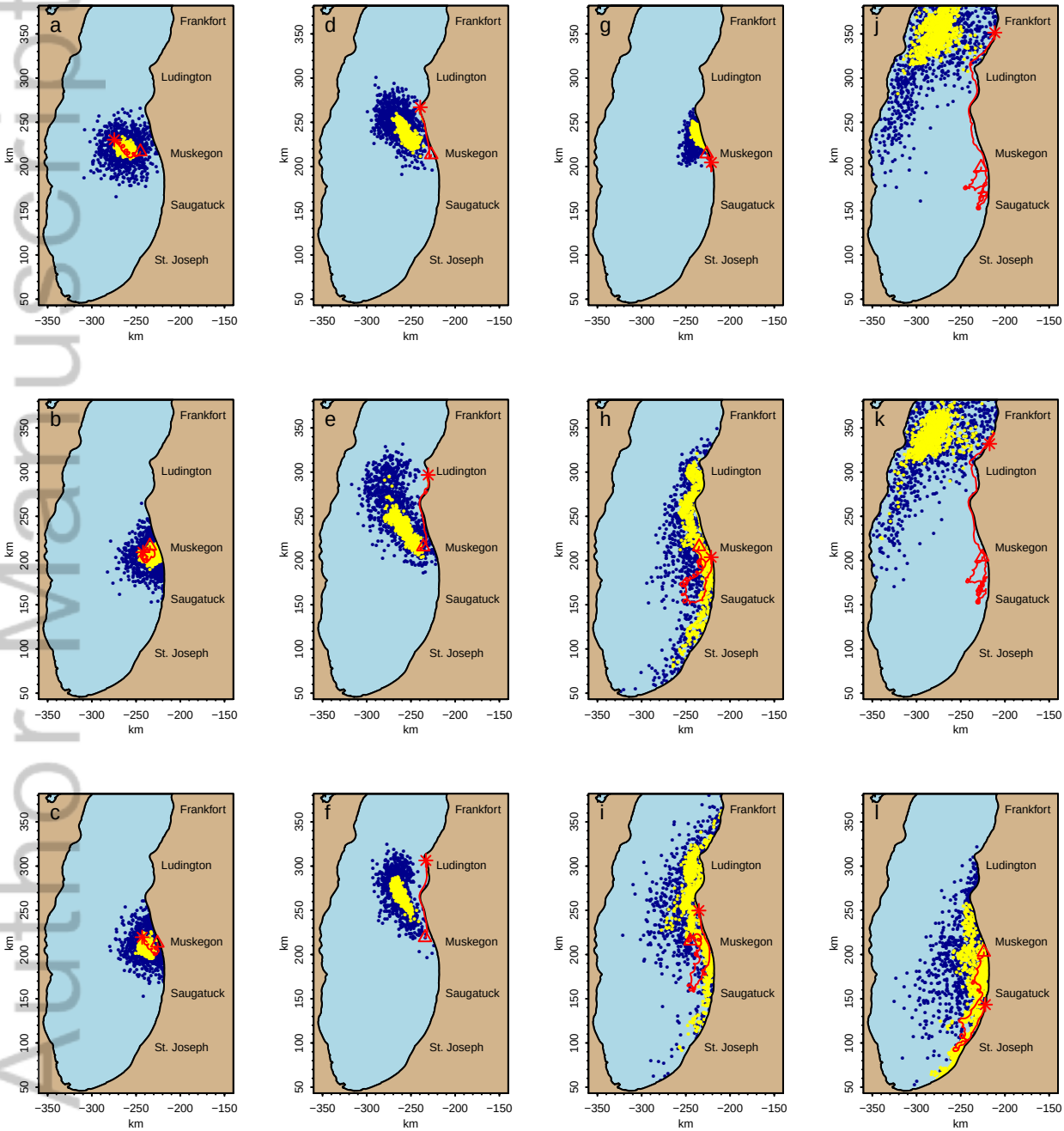

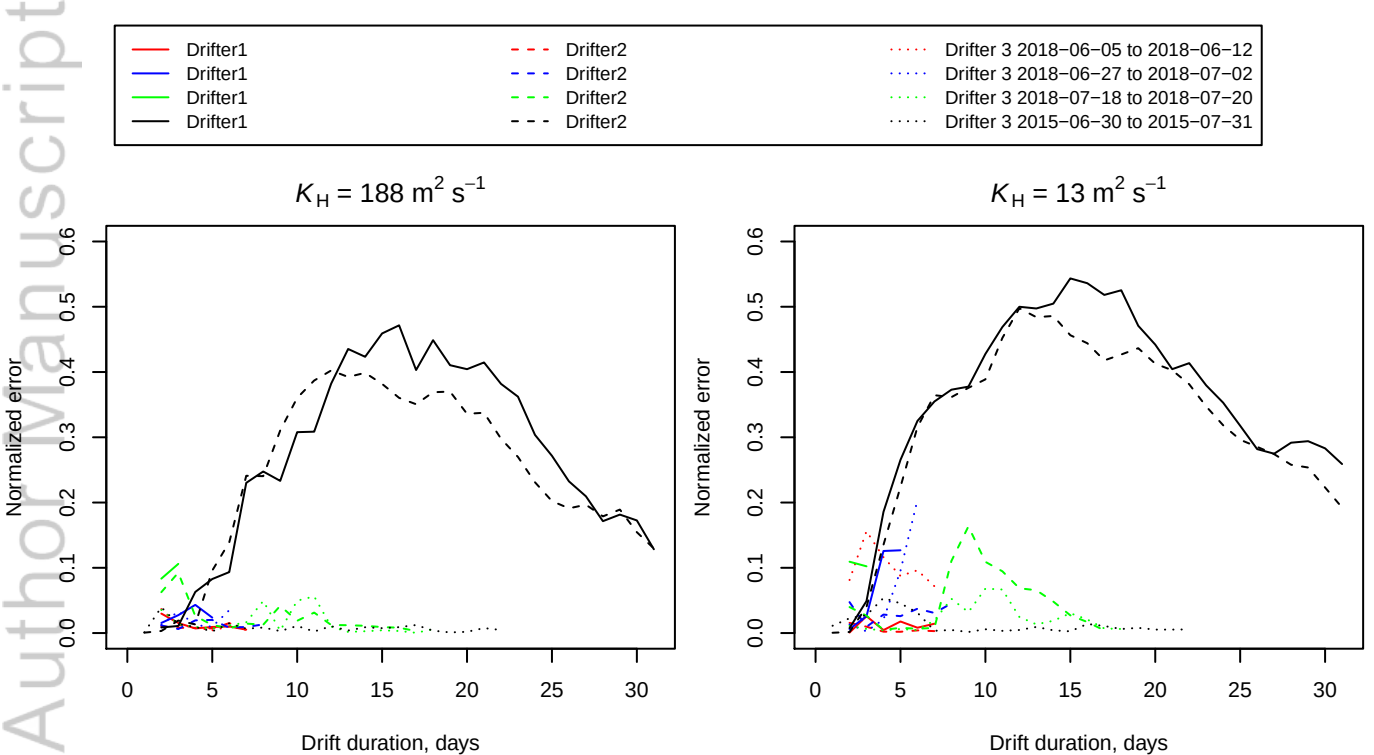

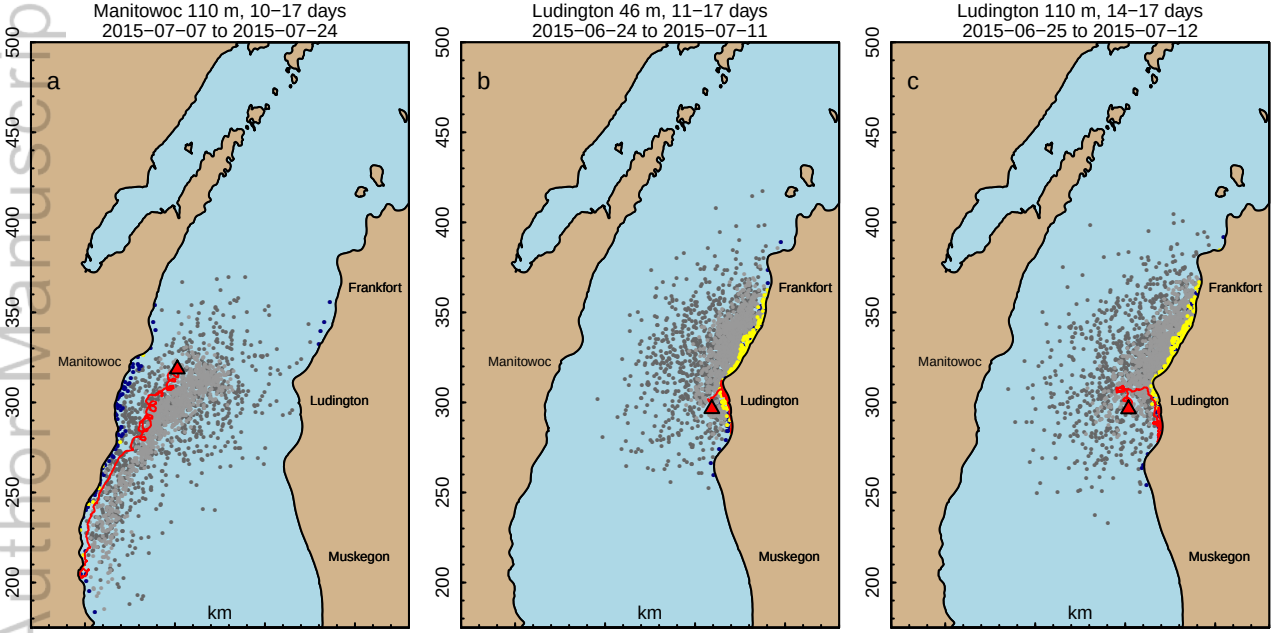

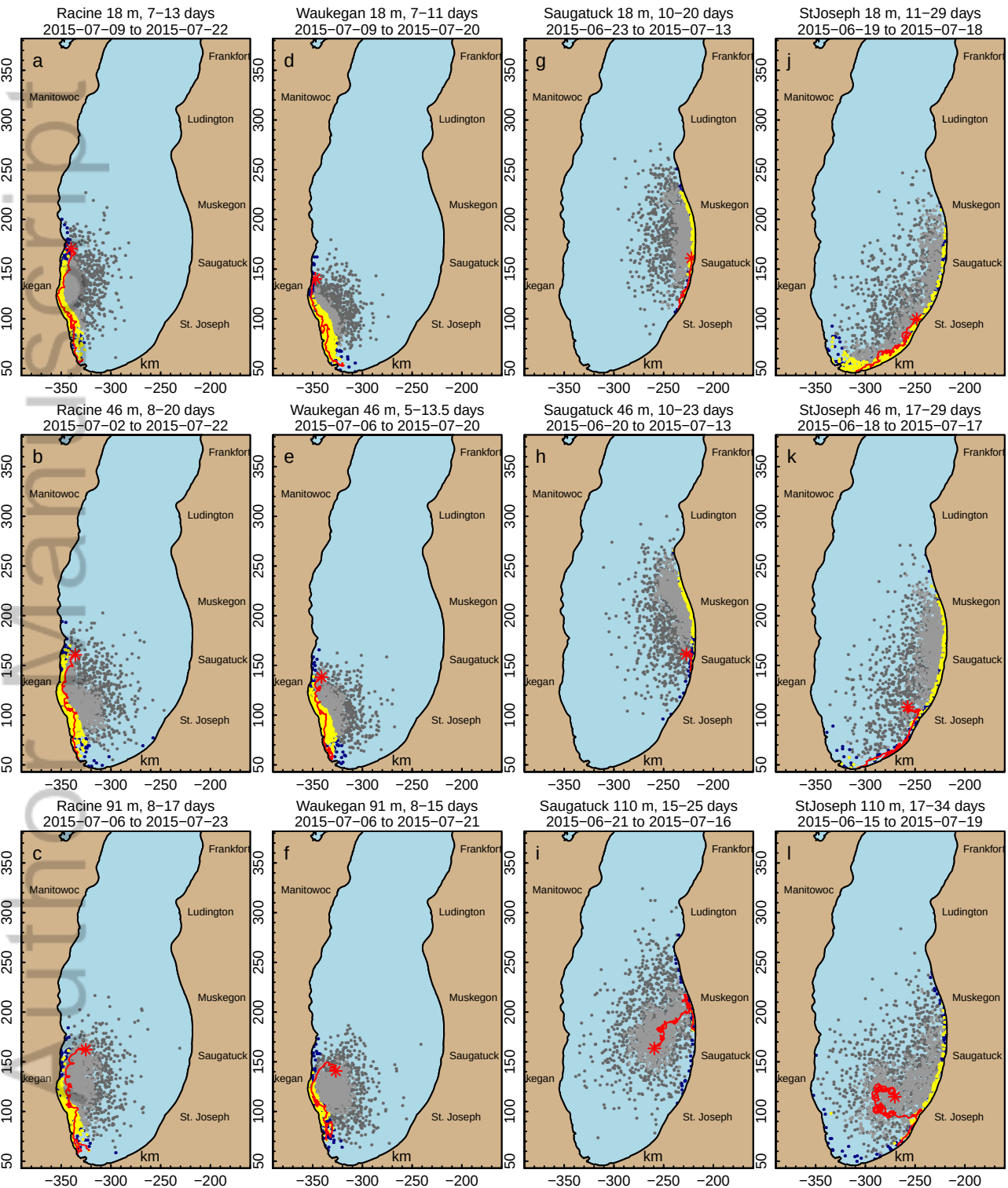
Racine 18 m, 7–13 days
2015–07–09 to 2015–07–22
Waukegan 18 m, 7–11 days
2015–07–09 to 2015–07–20
Saugatuck 18 m, 10–20 days
2015–06–23 to 2015–07–13
StJoseph 18 m, 11–29 days
2015–06–19 to 2015–07–18
Racine 46 m, 8–20 days
2015–07–02 to 2015–07–22
Waukegan 46 m, 5–13.5 days
2015–07–06 to 2015–07–20
Saugatuck 46 m, 10–23 days
2015–06–20 to 2015–07–13
StJoseph 46 m, 17–29 days
2015–06–18 to 2015–07–17
Racine 91 m, 8–17 days
2015–07–06 to 2015–07–23
Waukegan 91 m, 8–15 days
2015–07–06 to 2015–07–21
Saugatuck 110 m, 15–25 days
2015–06–21 to 2015–07–16
StJoseph 110 m, 17–34 days
2015–06–15 to 2015–07–19
a
b
c
d
e
f
g
h
i
j
k
l
Manitowoc
Frankfort
Ludington
Muskegon
Saugatuck
St. Joseph
km
50
100
150
200
250
300
350
−350
−300
−250
−200
K_H = 13 m^2 s^{-1}
K_H = 188 m^2 s^{-1}